

# The low-rank tensor-train finite difference method for three-dimensional parabolic equations

Gianmarco Manzini<sup>1</sup> and Tommaso Sorgente<sup>2</sup>

<sup>1</sup>T-5, Theoretical Division, Los Alamos National Laboratory, Los Alamos, NM, USA

<sup>2</sup>Istituto di Matematica Applicata e Tecnologie Informatiche “Enrico Magenes”, Consiglio Nazionale delle Ricerche, Genova, Italy

## Abstract

This paper presents a numerical framework for the low-rank approximation of the solution to three-dimensional parabolic problems. The key contribution of this work is the tensorization process based on a tensor-train reformulation of the second-order accurate finite difference method. We advance the solution in time by combining the finite difference method with an explicit and implicit Euler method and with the Crank-Nicolson method. We solve the linear system arising at each time step from the implicit and semi-implicit time-marching schemes through a matrix-free preconditioned conjugate gradient (PCG) method, appositely designed to exploit the separation of variables induced by the tensor-train format. We assess the performance of our method through extensive numerical experimentation, demonstrating that the tensor-train design offers a robust and highly efficient alternative to the traditional approach. Indeed, the usage of this type of representation leads to massive time and memory savings while guaranteeing almost identical accuracy with respect to the traditional one. These features make the method particularly suitable to tackle challenging high-dimensional problems.

## 1 Introduction

We consider the three-dimensional, open, bounded, hyper-rectangular domain  $\Omega \subset \mathbb{R}^3$  with boundary  $\Gamma = \partial\Omega$ . We are interested in the numerical approximation to the solution  $u$  of the parabolic equation with Dirichlet boundary condition:

$$\begin{aligned} \frac{\partial u}{\partial t} - \Delta u &= f && \text{in } \Omega \times (0, T], \\ u &= g && \text{on } \Gamma \times (0, T], \end{aligned} \quad (1)$$

where  $f$  and  $g$  on the right-hand side of (1) are the forcing term and the Dirichlet boundary function, respectively. To complete the mathematical model, we assume that  $u$  at the initial time  $t = 0$  satisfies the condition:

$$u(\cdot, 0) = u_0 \quad \text{in } \bar{\Omega}, \quad (2)$$

where  $\bar{\Omega}$  is the closure of  $\Omega$  in  $\mathbb{R}^3$ . Under suitable regularity assumption on  $f, g, u_0$ , and  $\Gamma$ , we can prove that the problem is well-posed [12]. Throughout this paper, we assume that the solution to (1) exists, is unique, and possesses sufficient regularity for all the approximations and estimates that follow to be meaningful.

Numerous approximation methods have been developed to solve such model problems, including *Finite Difference Methods (FDMs)* [34], *Finite Element Methods (FEMs)* [7], *Finite Volume Methods (FVMs)* [36], and *Spectral Methods* [13, 33]. Time integration typically employs explicit, implicit, or semi-implicit (Crank-Nicolson) schemes [23]. While implicit and semi-implicit methods offer better stability than explicit schemes, allowing larger time steps, they require solving linear systems at each time step, increasing the computational complexity.

## 1.1 A first step towards dual grid discretizations

In this work, we present a second-order accurate spatial discretization for problem (1)-(2), employing a *dual grid approximation* of  $u$  and its Laplacian,  $\Delta u$ , which combines both cell-centered and vertex-centered discretizations of these quantities. The dual grid approach offers several decisive advantages over traditional single grid methods that make it particularly suitable for tensor-train reformulations. First, dual grid discretizations eliminate spurious numerical oscillations that commonly plague single grid methods in fluid dynamics applications. As demonstrated in the pioneering work by Harlow and Welch [16], positioning velocity components at cell faces while maintaining pressure at cell centers creates natural pressure-velocity coupling that prevents checkerboard pressure modes without requiring artificial stabilization techniques. Second, dual grid methods achieve exact discrete conservation of fundamental physical quantities in fluid dynamics simulation, e.g., mass, momentum, and energy, at machine precision through their inherent geometric structure [27, 32]. This property, impossible to guarantee with interpolation-based single grid approaches, prevents unphysical solution drift and ensures long-term stability in time-dependent simulations. Third, Discrete Duality Finite Volume (DDFV) methods demonstrate remarkable robustness on non-orthogonal, anisotropic, and severely distorted meshes where traditional finite volume methods lose accuracy or fail entirely [5, 11]. Finally, dual grid discretizations achieve superior stability properties through their inherent mathematical structure, with rigorous analysis proving unconditional inf-sup stability for DDFV methods [6] and optimal convergence rates for mimetic methods on general polyhedral meshes [8].

As a first step towards a dual grid approximation of more complex application problems, such as those mentioned above, our approach for the parabolic equation utilizes hyper-rectangular grids that match the domain shape, maintaining two interconnected representations of the solution. One representation is defined at the vertices of the mesh (vertex-centered) containing the primary solution values, the other at the cell centers (cell-centered), providing a complementary approximation that facilitates more accurate discretization of differential operators. These two representations work together during the discretization process, where the information is transferred between them through carefully designed operators that preserve the overall accuracy of the scheme while creating a more robust numerical framework compared to single-grid methods. The discrete formulation of partial differential operations on this dual grid representation transforms cell-based unknowns into vertex-based unknowns (and vice versa), requiring specialized formulations of gradient, divergence, and Laplacian operators that maintain consistency across both representations and preserve important mathematical properties of the continuous differential operators. This hybrid spatial discretization is finally coupled with first-order explicit or implicit Euler schemes, or the second-order accurate semi-implicit Crank-Nicolson method for time integration [25]. Our methods ultimately yield an ODE system of the form:

$$\frac{du_v(\cdot; t)}{dt} = \Delta^v u_v(\cdot; t) + f(\cdot; t),$$

where  $\Delta^v u_v(\cdot; t)$  is the vertex Laplace term built by applying appropriate discretization formulas to  $u_v(\cdot; t)$ , while  $f(\cdot; t)$  is the source term evaluated at the mesh vertices at time  $t$ . The resulting schemes are second-order accurate in space and first-order or second-order accurate in time, depending on the chosen time-marching scheme.

## 1.2 Tensor-train format and related work

A conventional “full-grid” implementation of such schemes inevitably faces the *curse of dimensionality*, where memory and computational costs grow exponentially with the number of dimensions [3]. Even for three-dimensional problems, calculations become prohibitively expensive after a few mesh refinements. Our primary contribution is reformulating this finite difference/finite volume method into a more efficient algorithm using the low-rank tensor-train format to mitigate the curse of dimensionality.

The tensor-train (TT) format represents high-dimensional tensors as products of lower-dimensional TT cores, each associated with a spatial dimension [29]. For an  $N_v^x \times N_v^y \times N_v^z$  grid, the storage required by the TT representation scales as  $\mathcal{O}(Nr^2)$ , where  $N = \max(N_v^x, N_v^y, N_v^z)$  and  $r$  is the TT rank, compared to  $\mathcal{O}(N^3)$  for conventional approaches. When  $r \ll N$ , this scaling yields substantial savings in memory and computational cost. It is important to distinguish between the tensor-train format and the quantized tensor-train (QTT) format, which represents a distinct extension of TT. While TT operates directly on the original tensor dimensions, QTT introduces additional (often non-physical) dimensions through binary encoding of the original indices [19]. This distinction is crucial, as most existing literature focuses on either QTT-based approaches or applications to finite element methods rather than finite difference/finite volume methods for single and dual grid formulations.

Previous work on tensor methods for partial differential equations (PDEs) includes several distinct research directions. Several studies [17, 18, 26] have developed QTT-based finite element methods for elliptic problems, with applications to multiscale diffusion and curvilinear domains. These works primarily focus on steady-state equations rather than time-dependent problems. In Reference [9], both TT and QTT formats are applied to parabolic problems, particularly the Fokker-Planck equation, using alternating linear schemes (ALS) as their core numerical method. Their approach differs fundamentally from ours, which employs time-marching schemes directly on the TT cores. Several papers have explored Krylov subspace methods for linear systems with tensor product structure [2, 22, 31], including TT-GMRES [10] and general Krylov frameworks on low-rank tensor manifolds [21]. While these works provide important algorithmic foundations, they do not address the specific challenges of time-dependent parabolic problems in the TT format using finite difference discretizations. Various preconditioners have been developed for tensor-structured problems [1, 9], though most focus on general tensor formats or specific application domains rather than time-dependent parabolic problems with hybrid spatial discretizations.

### 1.3 Novel contributions

This work introduces several novel contributions that advance the state-of-the-art in tensor-based numerical methods for time-dependent PDEs. All of these contributions are developed within the tensor-train framework introduced by Oseledets [29]. In particular, our focus on finite difference/finite volume discretizations for time-dependent parabolic problems in the TT format presents unique challenges and opportunities that have not been previously addressed in the literature. Although we do not explore their potential application to the QTT framework, such extensions are expected to be straightforward in most cases and will be the focus of future research. We summarize the key contributions of this work as follows.

- (i) **Novel hybrid spatial discretization in TT format.** We present the first comprehensive framework that combines cell-centered and vertex-centered finite difference approximations within the tensor-train representation for three-dimensional parabolic problems. Unlike existing TT/QTT-based approaches, which typically focus on a single discretization type, our dual-grid methodology enables more flexible and accurate spatial approximations while maintaining the computational efficiency of the TT format. Unlike standard Laplace approximations represented by Kronecker sums of the form  $D^2 \otimes I \otimes \dots \otimes I + \dots + I \otimes \dots \otimes I \otimes D^2$ , where  $D^2 = (1/h) \text{tridiag}(-1, 2, -1)$ , our discretizations involve transformations between cell-based and vertex-based unknowns that require specialized reconstruction techniques and operators working directly on TT cores. This approach is related to the dual grid discretizations discussed previously. While we do not yet have a theoretical framework to analyze this methodology in the tensor-train framework, our numerical experiments demonstrate that the approach is *rank-stable*, preserving the rank of low-rank initial solutions through suitable rounding procedures in the time-marching method.
- (ii) **Extension to variable meshes and domain remapping.** We generalize our TT-based methodology to support non-uniform spatial discretizations and remapped domains, expanding the applicability of tensor-train methods beyond the uniform grid assumptions commonly found in the literature. This extension maintains second-order spatial accuracy while preserving the computational benefits of the TT representation.
- (iii) **Direct implementation of multiple time-stepping schemes on TT cores.** We redesign time-stepping algorithms—including explicit Euler, implicit Euler, and Crank-Nicolson schemes—to operate directly on the TT representation. This approach ensures computational efficiency across the entire time integration process by manipulating TT cores directly. Unlike previous approaches that rely on alternating linear schemes (ALS) [9], our methods implement classical time-marching schemes directly in the TT format, maintaining the mathematical structure of the original schemes while exploiting the computational advantages of the TT representation.
- (iv) **TT-specialized matrix-free preconditioned conjugate gradient method.** To solve the linear systems arising from implicit and semi-implicit time-stepping schemes, we reformulate the preconditioned conjugate gradient (PCG) algorithm to operate directly on the TT cores of the Krylov direction vectors. To this end, we employ a *matrix-free formulation* of the matrix-vector product, so that the latter is provided by an application of the discrete time operator to the Krylov directions. Practically, we never build the time operator as a matrix in any given full or tensor-compressed format. This approach offers two key advantages:
  - eliminates the need to convert Krylov direction vectors into full tensor representations during the iterative process;
  - avoids the explicit assembly or construction of the system matrix in both full and approximate TT representations, significantly reducing computational and memory overhead.

To complete the PCG algorithm, we propose a specialized preconditioner that acts directly on the TT cores by leveraging univariate finite difference operators and exploiting the separable structure of the discretization. While previous works have explored preconditioners for tensor-structured problems [1, 9], our approach is specifically designed for the discrete operators arising from our hybrid spatial discretization and focuses on maintaining rank stability throughout the solution process. By bypassing the explicit construction of the system matrix in TT format, the method preserves the low-rank structure throughout the preconditioning and solution process, while achieving optimal computational scaling with refinement in space and time.

(v) **Comprehensive algorithmic framework.** We provide a complete algorithmic description, including a detailed analysis of computational complexity, memory requirements, and numerical accuracy. In particular, we demonstrate that our TT reformulation preserves the second-order accuracy of the hybrid finite difference approximation, thereby ensuring theoretical guarantees for spatial and temporal accuracy within the TT framework. We also carefully describe technical implementation details, such as the setting of the boundary conditions, or the choice of threshold values, making it easy to implement our algorithms and replicate our results.

In summary, the combination of these contributions results in substantial practical improvements: memory requirements scale as  $\mathcal{O}(Nr^2)$  instead of  $\mathcal{O}(N^3)$  for traditional methods, where  $N$  is the grid size per dimension and  $r$  is the TT rank. For problems where  $r \ll N$ , this represents *orders-of-magnitude improvements in both memory usage and computational time*, making previously intractable three-dimensional parabolic problems computationally feasible. This methodology opens new possibilities for solving large-scale multidimensional problems in the area of finite difference/finite volume methods that were previously computationally prohibitive with conventional approaches.

## 1.4 Paper’s outline

The remainder of this paper is organized as follows: Section 2 presents the fundamental mathematical framework, introducing the notation and essential concepts of the tensor-train format that underpins our methodology. Section 3 develops the finite difference/finite volume discretization scheme and its reformulation within the tensor-train framework for the numerical approximation of the system defined by Equation (1). In Section 4, we generalize our approach by extending the discretization method to handle problems on variable mesh sizes and remapped domains, maintaining the framework established in Section 3. Section 5 details the implementation of the different time marching techniques, including the preconditioned conjugate gradient method for solving the linear systems that arise from implicit and semi-implicit time discretizations. Section 6 demonstrates the effectiveness and efficiency of our proposed methodology through comprehensive numerical experiments and performance analysis. Section 7 summarizes our findings, discusses their implications, and outlines potential directions for future research.

## 2 Tensor-train format: notation, basic definitions, background properties

We shortly recall here some notation, basic definitions, and a few technicalities about tensors and the tensor-train format, referring to the review article [20] and the pioneering papers [29, 30] for a detailed exposition. A  $d$ -dimensional tensor  $\mathcal{A}$  is a multi-dimensional array with  $d$  indices, e.g.,  $\mathcal{A} = (\mathcal{A}(i_1, i_2, \dots, i_d))$ ,  $i_\ell = 1, 2, \dots, n_\ell$ ,  $\ell = 1, 2, \dots, d$ . Since we are interested in solving three-dimensional (3D) problems, we restrict all basic definitions to  $0 \leq d \leq 3$ , and use the Latin indices  $i, j, k$  instead of  $i_1, i_2, i_3$ . Technically, scalar quantities, vectors, and matrices are special cases of  $d$ -way tensors for  $d = 0, 1, 2$ , respectively, but throughout the paper, we prefer to use a distinct notation for them for clarity of exposition. We denote a *scalar quantity* using normal, lower-case fonts, e.g.  $a, b, c$ , etc; a *vector field* using bold, lower-case fonts, e.g.,  $\mathbf{a}, \mathbf{b}, \mathbf{c}$ , etc; a *matrix* using normal, upper case fonts, e.g.  $A, B, C$ , etc; a *3-dimensional tensor* using calligraphic, upper case fonts, e.g.,  $\mathcal{A}, \mathcal{B}, \mathcal{C}$ , etc. We address the entries of  $d$ -dimensional quantities for  $d \geq 1$  by using a MATLAB-like notation; accordingly, the symbol “:” denotes a *free index*. So,  $a(i)$ ,  $A(i, j)$ ,  $\mathcal{A}(i, j, k)$  are the  $i$ -th component of vector  $\mathbf{a}$ , the  $(i, j)$ -th component of matrix  $A$ , and the  $(i, j, k)$ -th component of tensor  $\mathcal{A}$ , respectively.

It is convenient to introduce the concepts of *fibers* and *slices*. A fiber is the vector that we obtain from a tensor by fixing all indices but one; a slice is the matrix that we obtain by fixing all indices but two. Therefore, a 3D tensor  $\mathcal{A}(i, j, k)$  has three distinct fibers, e.g.,  $\mathcal{A}(:, j, k)$ ,  $\mathcal{A}(i, :, k)$ , and  $\mathcal{A}(i, j, :)$ , and three distinct slices, e.g.,  $\mathcal{A}(i, :, :)$ ,  $\mathcal{A}(:, j, :)$ , and  $\mathcal{A}(:, :, k)$ .

We say that a 3D tensor  $\mathcal{A} \in \mathbb{R}^{n_1 \times n_2 \times n_3}$  is in *tensor-train format* if there exist three 3D tensors, called *tensor-train cores* and denoted by  $\mathcal{A}_\ell \in \mathbb{R}^{r_{\ell-1} \times n_\ell \times r_\ell}$ , for  $\ell = 1, 2, 3$  and with  $r_0 = r_3 = 1$ , such that

$$\mathcal{A}(i, j, k) = \sum_{\alpha_1=1}^{r_1} \sum_{\alpha_2=1}^{r_2} \mathcal{A}_1(i, \alpha_1) \mathcal{A}_2(\alpha_1, j, \alpha_2) \mathcal{A}_3(\alpha_2, k). \quad (3)$$

Since  $r_0 = r_3 = 1$ , the two cores  $\mathcal{A}_1$  and  $\mathcal{A}_3$  are indeed matrices, so we write them with two indices in (3), but still keeping the tensor notation. We can reformulate definition (3) by introducing three slice matrices  $A_1(i) = \mathcal{A}_1(:, i, :) \in \mathbb{R}^{r_0 \times r_1}$ ,  $A_2(j) = \mathcal{A}_2(:, j, :) \in \mathbb{R}^{r_1 \times r_2}$ , and  $A_3(k) = \mathcal{A}_3(:, k, :) \in \mathbb{R}^{r_2 \times r_3}$ , which are parametrized with the spatial indices  $i, j$ , and  $k$ , such that

$$\mathcal{A}(i, j, k) = A_1(i) A_2(j) A_3(k),$$

for every possible combination of the indices  $i, j, k$ . The integers  $r_1, r_2$  represent the *TT ranks* of  $\mathcal{A}$ , that is, the internal sizes of tensors  $\mathcal{A}_1, \mathcal{A}_2, \mathcal{A}_3$ . It is also convenient to define an upper bound of these ranks as  $r = \max \{r_\ell\}_\ell$ .

In the next section, we will introduce two distinct types of 3D tensors, which are logically associated with the vertices and the cells of a 3D mesh, respectively. To emphasize the nature of such tensors, instead of  $(i, j, k)$  we will use the index triple  $(i_v, j_v, k_v)$  in the first case, and the index triple  $(i_c, j_c, k_c)$  in the second. This double index notation of vertices and cells avoids using “half-indices”; usually, we might denote two consecutive vertices as, for example, “ $i$ ” and “ $i + 1$ ” along the X direction and the cell between them as “ $i + \frac{1}{2}$ ”. However, this notation is very cumbersome when we need to index the cores of the tensor-train representation of a cell grid function as these indices should be integers and not half integers. For this reason, we prefer using this double-index notation, which is completely equivalent to the more familiar one once we observe that the  $i_v$ -th vertex and the  $i_c$ -th cell correspond to the  $i$ -th vertex and the  $(i + \frac{1}{2})$ -th cell, respectively, if we assume that  $i = i_v = i_c$ , as it is discussed in the next section.

A very efficient tensor-train decomposition algorithm called TT-SVD is available from Ref. [29], which is based on a sequence of Singular Value Decomposition (SVD) of auxiliary matrices. The most crucial properties of this algorithm are those related to the TT ranks and the ranks of the so-called *matrix unfoldings*. A three-dimensional tensor has two distinct matrix unfoldings. The first unfolding is the matrix  $A_1 \in \mathbb{R}^{n_1 \times (n_2 n_3)}$  whose row index corresponds to the first tensor index  $i$ , and whose column index is a bijective remap, say  $\eta_1$ , of the tensor indices  $(j, k)$ , so that  $A_1(i, \eta_1(j, k)) = \mathcal{A}(i, j, k)$ . The second unfolding is the matrix  $A_2 \in \mathbb{R}^{(n_1 n_2) \times n_3}$  whose row index is a bijective remap, say again  $\eta_2$ , of the tensor indices  $(i, j)$ , and column index is equal to  $k_v$  so that  $A_2(\eta_2(i, j), k) = \mathcal{A}(i, j, k)$ .

According to [29, Theorem 2.1], TT-SVD can compute an exact representation of the tensor  $\mathcal{A}$  in the TT format with TT ranks  $r_\ell$  satisfying  $r_\ell = \text{rank}(A_\ell)$  for both  $\ell = 1, 2$ . According to [29, Corollary 2.4], if we select smaller ranks  $r'_\ell \leq \text{rank}(A_\ell)$ , then the best approximation

$$\mathcal{A}_{\text{best}}^{TT} = \arg \inf_{\mathcal{A}^{TT} \in \mathbb{TT}(\mathbf{r}'_\ell)} \|\mathcal{A} - \mathcal{A}^{TT}\|_{\mathcal{F}}$$

in the TT format of  $\mathcal{A}$  exists with such  $r'_\ell$  as internal ranks. Here, the *infimum* is taken over the set of tensors  $\mathbb{TT}(\mathbf{r}'_\ell)$  in tensor-train format having internal ranks  $\mathbf{r}'_\ell = (r'_1, r'_2)$ . The TT-SVD algorithm balances computational efficiency and approximation quality since it returns a *quasi-optimal best approximation*  $\mathcal{A}^{TT}$  in the sense that

$$\|\mathcal{A} - \mathcal{A}^{TT}\|_{\mathcal{F}} \leq C_{TT}(d) \|\mathcal{A} - \mathcal{A}_{\text{best}}^{TT}\|_{\mathcal{F}}.$$

For  $d = 3$ , the inequality constant is  $C_{TT} = \sqrt{2}$  since the general expression is  $C_{TT}(d) = \sqrt{d-1}$  [30].

Multi-linear algebra operations, such as addition, multiplication by a scalar, element-wise (Hadamard) multiplication, contraction with matrices and vectors are possible through a straightforward implementation that facilitates tensor calculations [29]. However, these operations may increase the TT ranks, and an application of the so-called *rounding* algorithm [29] is required to control the rank growth. We denote this operation with the symbol  $\text{rndg}(\cdot)$ . Included in the  $\text{rndg}$  procedure, there is a threshold  $\epsilon$  which ensures that the “rounded” tensor-train will approximate the original one accurately. The choice of  $\epsilon$  is crucial for the good behavior of the method. Smaller  $\epsilon$  values lead to higher TT ranks, resulting in more accurate but more expensive computations, and vice versa.

A sampling algorithm based on the MaxVol row and column selection strategy [15] is available for constructing an approximate representation of a tensor in the TT format without precomputing and storing the tensor, see, e.g., [30]. We use this algorithm to ensure efficient processing to the treatment of the right-hand side term  $f$ .

### 3 Tensor-train reformulation of finite difference operators on 3D cartesian grids

In this section, we focus exclusively on the spatial discretization. Therefore, for clarity and simplicity, we will omit the time dependence of spatially varying fields, i.e., we will discretize  $u(\mathbf{x})$  and its derivatives in space instead of  $u(\mathbf{x}, t)$ .

#### 3.1 Regular equispaced meshes and grid functions

We consider the computational domain  $\Omega = (a_x, b_x) \times (a_y, b_y) \times (a_z, b_z)$ , for the three pairs of real values  $a_\ell$  and  $b_\ell$ , with  $-\infty < a_\ell < b_\ell < \infty$ ,  $\ell \in \{x, y, z\}$ . We partition  $\Omega$  along the directions X, Y and Z with constant mesh size steps  $h_x, h_y, h_z$ , respectively, and set the “characteristic mesh size”  $h = \min(h_x, h_y, h_z)$ . This partitioning introduces  $N_v^x$ ,  $N_v^y$ , and  $N_v^z$  vertices and  $N_c^x = N_v^x - 1$ ,  $N_c^y = N_v^y - 1$ ,  $N_c^z = N_v^z - 1$  univariate closed intervals along X, Y and Z, respectively. The mesh size steps satisfy the conditions:  $N_c^x h_x = b_x - a_x$ ,  $N_c^y h_y = b_y - a_y$ , and  $N_c^z h_z = b_z - a_z$ .

We label each mesh vertex with the index triple  $(i_v, j_v, k_v)$ , so that the  $(i_v, j_v, k_v)$ -th vertex, also denoted as  $v(i_v, j_v, k_v)$ , has coordinates  $\mathbf{x}_v = (x_v(i_v), y_v(j_v), z_v(k_v))$ , where

$$\begin{aligned} x_v(i_v) &= a_x + i_v h_x & \text{for } i_v = 0, 1, \dots, N_v^x - 1, \\ y_v(j_v) &= a_y + j_v h_y & \text{for } j_v = 0, 1, \dots, N_v^y - 1, \\ z_v(k_v) &= a_z + k_v h_z & \text{for } k_v = 0, 1, \dots, N_v^z - 1. \end{aligned}$$

We label each mesh cell with the index triple  $(i_c, j_c, k_c)$ , so that the  $(i_c, j_c, k_c)$ -th cell, also denoted as  $c(i_c, j_c, k_c)$ , is given by the tensor product of the univariate closed intervals along X, Y and Z

$$\begin{aligned} c(i_c, j_c, k_c) &= [x_v(i_v, j_v, k_v), x_v(i_v + 1, j_v, k_v)] \times [y_v(i_v, j_v, k_v), y_v(i_v, j_v + 1, k_v)] \times \\ &\quad \times [z_v(i_v, j_v, k_v), z_v(i_v, j_v, k_v + 1)]. \end{aligned}$$

Cell indices run as  $i_c = 0, 1, \dots, N_c^x - 1$ ,  $j_c = 0, 1, \dots, N_c^y - 1$ ,  $k_c = 0, 1, \dots, N_c^z - 1$ . Cell  $c(i_c, j_c, k_c)$  can also be defined as the convex envelope of its eight vertices:

$$\begin{aligned} c(i_c, j_c, k_c) &= \text{convex envelope of} \\ &\quad \left\{ v(i_v, j_v, k_v), v(i_v, j_v + 1, k_v), v(i_v, j_v + 1, k_v + 1), v(i_v, j_v, k_v + 1), \right. \\ &\quad \left. v(i_v + 1, j_v, k_v), v(i_v + 1, j_v + 1, k_v), v(i_v + 1, j_v + 1, k_v + 1), v(i_v + 1, j_v, k_v + 1) \right\}. \end{aligned} \quad (4)$$

Consequently, we can identify cell  $c(i_c, j_c, k_c)$  as the cell whose “first” vertex in definition (4) is  $v(i_v, j_v, k_v)$ , provided that  $i_v = i_c$ ,  $j_v = j_c$ , and  $k_v = k_c$ . This fact introduces a precise and well-defined bijective correspondence between the vertex and the cell numbering systems. The cell center has coordinates  $\mathbf{x}_c = (x_c(i_c), y_c(j_c), z_c(k_c))$ , where

$$\begin{aligned} x_c(i_c) &= a_x + \left(i_c + \frac{1}{2}\right) h_x = \frac{x(i_v) + x(i_v + 1)}{2}, \\ y_c(j_c) &= a_y + \left(j_c + \frac{1}{2}\right) h_y = \frac{y(j_v) + y(j_v + 1)}{2}, \\ z_c(k_c) &= a_z + \left(k_c + \frac{1}{2}\right) h_z = \frac{z(k_v) + z(k_v + 1)}{2}. \end{aligned}$$

We represent a scalar field  $u(x, y, z)$  as a *vertex grid function*  $u_v = (u_v(i_v, j_v, k_v))$  or a *cell grid function*  $u_c = (u_c(i_c, j_c, k_c))$ . These grid functions are three-dimensional tensors regardless of being associated with vertices or cells. Depending on the context, we may interpret each value  $u_v(i_v, j_v, k_v)$  as either  $u(\mathbf{x}_v)$ , i.e., the value of  $u(\mathbf{x})$  sampled at the  $(i_v, j_v, k_v)$ -th vertex with coordinates  $\mathbf{x}_v$ , or as an approximation of it. Similarly, we may interpret each value  $u_c(i_c, j_c, k_c)$  as either  $u(\mathbf{x}_c)$ , i.e., the value of  $u(\mathbf{x})$  sampled at the center of the  $(i_c, j_c, k_c)$ -th cell with coordinates  $\mathbf{x}_c$ , or as an approximation of it. A second interpretation is also possible where this quantity is either the cell average or an approximation of the cell average of  $u(\mathbf{x})$  over cell  $c(i_c, j_c, k_c)$ . The first interpretation is related to a finite difference

setting, the second one to a finite volume setting, but on orthogonal, cartesian grids, they are equivalent up to an error scaling like  $\mathcal{O}(h^2)$ , and may eventually lead to the same approximation formulas. Throughout this paper, we leave the interpretation of  $u_c(i_c, j_c, k_c)$  unspecified, thus referring implicitly to both, although sometimes it may look like we have some preference for the finite difference one as we often implicitly refer to the concept of a “pointwise stencil”.

### 3.2 First derivatives of vertex grid functions

In our setting, the discrete derivative of a vertex grid function is a cell grid function. Let  $\partial_x^c u_v$ ,  $\partial_y^c u_v$ , and  $\partial_z^c u_v$  denote the three components of the discrete gradient of the grid function  $u_v$ . They are associated with cell  $c(i_c, j_c, k_c)$  and defined as follows:

$$\partial_x^c u_v(i_c, j_c, k_c) := \frac{1}{4h_x} \sum_{n=0}^1 \sum_{p=0}^1 \left( u_v(i_v + 1, j_v + n, k_v + p) - u_v(i_v, j_v + n, k_v + p) \right), \quad (5)$$

$$\partial_y^c u_v(i_c, j_c, k_c) := \frac{1}{4h_y} \sum_{m=0}^1 \sum_{p=0}^1 \left( u_v(i_v + m, j_v + 1, k_v + p) - u_v(i_v + m, j_v, k_v + p) \right), \quad (6)$$

$$\partial_z^c u_v(i_c, j_c, k_c) := \frac{1}{4h_z} \sum_{m=0}^1 \sum_{n=0}^1 \left( u_v(i_v + m, j_v + n, k_v + 1) - u_v(i_v + m, j_v + n, k_v) \right). \quad (7)$$

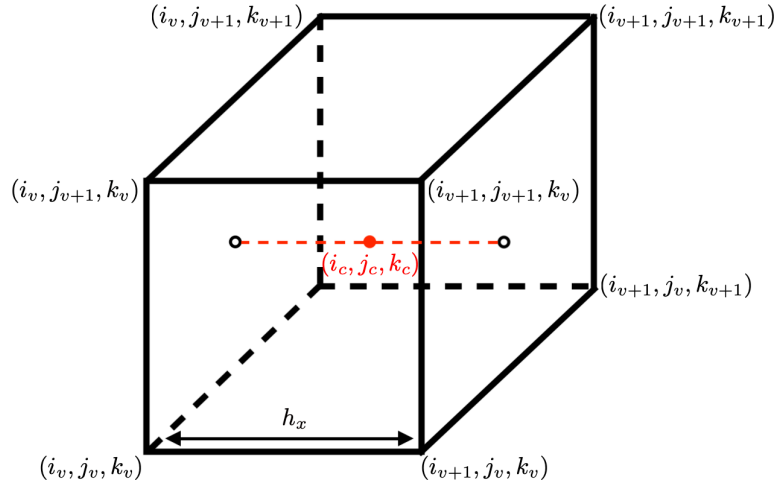


Figure 1: Computation of  $\partial_x^c u_v(i_c, j_c, k_c)$ .

Note that the difference operations are applied to the vertex indices, but the result is associated with the cell identified by taking  $i_c = i_v$ ,  $j_c = j_v$ ,  $k_c = k_v$  according to the numbering system of cells and vertices introduced in Section 3.1, see Figure 1. The association to a cell is reflected by the superscript “c” in the discrete difference operators  $\partial_x^c$ ,  $\partial_y^c$ , and  $\partial_z^c$ . Then, assuming that  $u_v(i_v + m, j_v + n, k_v + p) = u(x_v(i_v + m), y_v(j_v + n), z_v(k_v + p))$  with  $m, n, p = 0, 1$ , a straightforward Taylor expansion implies that

$$\begin{aligned} \left( \frac{\partial u}{\partial x} \right)_c &= \partial_x^c u_v(i_c, j_c, k_c) + \mathcal{O}(h^2), & \left( \frac{\partial u}{\partial y} \right)_c &= \partial_y^c u_v(i_c, j_c, k_c) + \mathcal{O}(h^2), \\ \left( \frac{\partial u}{\partial z} \right)_c &= \partial_z^c u_v(i_c, j_c, k_c) + \mathcal{O}(h^2), \end{aligned} \quad (8)$$

where, to ease the notation, the symbols  $(\partial u / \partial x)_c$ ,  $(\partial u / \partial y)_c$ , and  $(\partial u / \partial z)_c$  denote the corresponding first derivatives evaluated at the cell center  $(x_c(i_c), y_c(j_c), z_c(k_c))$ . We report the details of this calculation in A.

Formulas (5), (6), and (7) are rather standard in the finite difference and finite volume literature. However, they suffer the curse of dimensionality as the computational complexity of computing  $\partial_x^c u_v$ ,  $\partial_y^c u_v$ , and  $\partial_z^c u_v$  on a 3D,  $(N_v^x \times N_v^y \times N_v^z)$ -sized grid scales like  $\mathcal{O}(N^3)$  with  $N = \max(N_v^x, N_v^y, N_v^z)$  as already noted in the introduction. This “bad” scaling makes calculations expensive and almost unfeasible even for relatively small values of  $N$ , e.g., between  $10^2$  and  $10^3$ . Herein, we are interested in reformulating such first derivatives in the tensor-train format. Let

$$u_v^{TT}(i_v, j_v, k_v) = \sum_{\alpha_1=1}^{r_1} \sum_{\alpha_2=1}^{r_2} \mathcal{U}_1(i_v, \alpha_1) \mathcal{U}_2(\alpha_1, j_v, \alpha_2) \mathcal{U}_3(\alpha_2, k_v) = U_1(i_v) U_2(j_v) U_3(k_v)$$

be the TT representation of the grid function  $u_v$ , using cores  $\mathcal{U}_\ell$  and matrix slices  $U_\ell$  for  $\ell = 1, 2, 3$  according to the notation and definitions discussed in Section 2. At the moment, we do not need to specify if this is an “exact” or an “approximate” representation, nor if we obtained the grid function  $u_v$  (represented as  $u_v^{TT}$ ) by sampling some smooth function  $u(\mathbf{x})$  at the vertices of a given grid, or if  $u_v$  is the result of some complex calculations. For convenience of exposition, we assume that this is an exact representation so that it holds that  $u_v(i_v, j_v, k_v) = u_v^{TT}(i_v, j_v, k_v)$  for every meaningful index triple  $(i_v, j_v, k_v)$ . To compute the first derivative of  $u_v$  along the direction  $X$  in the TT format, i.e., the cell grid function  $\partial_x^c u_v^{TT}(i_c, j_c, k_c)$ , we apply definition (5), and we find that

$$\partial_x^c u_v^{TT}(i_c, j_c, k_c) := \frac{1}{4h_x} \sum_{n=0}^1 \sum_{p=0}^1 \left( u_v^{TT}(i_v + 1, j_v + n, k_v + p) - u_v^{TT}(i_v, j_v + n, k_v + p) \right). \quad (9)$$

Then, we expand the first summation on the right of (9), and using the tensor-train definition, we rewrite it as

$$\begin{aligned} \sum_{n=0}^1 \sum_{p=0}^1 u_v^{TT}(i_v + 1, j_v + n, k_v + p) &= u_v^{TT}(i_v + 1, j_v, k_v) + u_v^{TT}(i_v + 1, j_v + 1, k_v) \\ &\quad + u_v^{TT}(i_v + 1, j_v + 1, k_v + 1) + u_v^{TT}(i_v + 1, j_v, k_v + 1) \\ &= U_1(i_v + 1) U_2(j_v) U_3(k_v) + U_1(i_v + 1) U_2(j_v + 1) U_3(k_v) + U_1(i_v + 1) U_2(j_v + 1) U_3(k_v + 1) \\ &\quad + U_1(i_v + 1) U_2(j_v) U_3(k_v + 1) \\ &= U_1(i_v + 1) \left( U_2(j_v) + U_2(j_v + 1) \right) \left( U_3(k_v) + U_3(k_v + 1) \right). \end{aligned}$$

We repeat the same calculation for the second summation term on the right of Eq. (9), we take the difference between them and substitute the result into Eq. (9). We find that

$$\begin{aligned} \partial_x^c u_v^{TT}(i_c, j_c, k_c) &= U_1^x(i_c) U_2^x(j_c) U_3^x(k_c) \\ &:= \left( \frac{U_1(i_v + 1) - U_1(i_v)}{h_x} \right) \left( \frac{U_2(j_v) + U_2(j_v + 1)}{2} \right) \left( \frac{U_3(k_v) + U_3(k_v + 1)}{2} \right), \end{aligned}$$

where we identify the vertex index pairs  $(i_v, i_v + 1)$ ,  $(j_v, j_v + 1)$ ,  $(k_v, k_v + 1)$ , with the cell indices  $i_c, j_c, k_c$ , and the cores  $U_1^x, U_2^x$  and  $U_3^x$  parametrized with  $(i_c, j_c, k_c)$  with the cores of the first derivative of  $u_v^{TT}$  along the direction  $X$ . The superscript “ $x$ ” in the core symbols  $U_\ell^x$ ,  $\ell = 1, 2, 3$  refers to the direction of the derivative. We can similarly write the other two derivatives:

$$\begin{aligned} \partial_y^c u_v^{TT}(i_c, j_c, k_c) &= U_1^y(i_c) U_2^y(j_c) U_3^y(k_c) \\ &:= \left( \frac{U_1(i_v) + U_1(i_v + 1)}{2} \right) \left( \frac{U_2(j_v + 1) - U_2(j_v)}{h_y} \right) \left( \frac{U_3(k_v) + U_3(k_v + 1)}{2} \right), \end{aligned}$$

and

$$\begin{aligned} \partial_z^c u_v^{TT}(i_c, j_c, k_c) &= U_1^z(i_c) U_2^z(j_c) U_3^z(k_c) \\ &:= \left( \frac{U_1(i_v) + U_1(i_v + 1)}{2} \right) \left( \frac{U_2(j_v) + U_2(j_v + 1)}{2} \right) \left( \frac{U_3(k_v + 1) - U_3(k_v)}{h_z} \right). \end{aligned}$$

A crucial point of this construction is that no additional errors are introduced in the TT representation of the derivatives other than those of the finite difference approximation as in (8).



### 3.3 Second derivatives of vertex grid functions

To define the discrete second derivatives of  $u_v^{TT}$ , the vertex grid function  $u_v$  in the TT format representation, we proceed by still assuming that the TT representation is exact, i.e.,  $u_v^{TT}(i_v, j_v, k_v) = u_v(i_v, j_v, k_v)$ , and using a similar argument as for the first derivatives. So, we first start from the discrete second derivative formulas for  $u_v$  at cell  $c(i_c, j_c, k_c)$  along X, Y and Z, which are given by

$$\partial_{xx}^c u_v(i_c, j_c, k_c) = \frac{1}{8h_x^2} \sum_{m=0}^3 \eta_m \sum_{n=0}^1 \sum_{p=0}^1 \xi_n \xi_p u_v(i_v - 1 + m, j_v + n, k_v + p), \quad (10)$$

$$\partial_{yy}^c u_v(i_c, j_c, k_c) = \frac{1}{8h_y^2} \sum_{m=0}^3 \eta_m \sum_{n=0}^1 \sum_{p=0}^1 \xi_n \xi_p u_v(i_v + n, j_v - 1 + m, k_v + p), \quad (11)$$

$$\partial_{zz}^c u_v(i_c, j_c, k_c) = \frac{1}{8h_z^2} \sum_{m=0}^3 \eta_m \sum_{n=0}^1 \sum_{p=0}^1 \xi_n \xi_p u_v(i_v + n, j_v + p, k_v - 1 + m), \quad (12)$$

where  $\xi_0 = -1, \xi_1 = 1, \eta_0 = \eta_3 = 1, \eta_1 = \eta_2 = -1$ , see Figure 2.

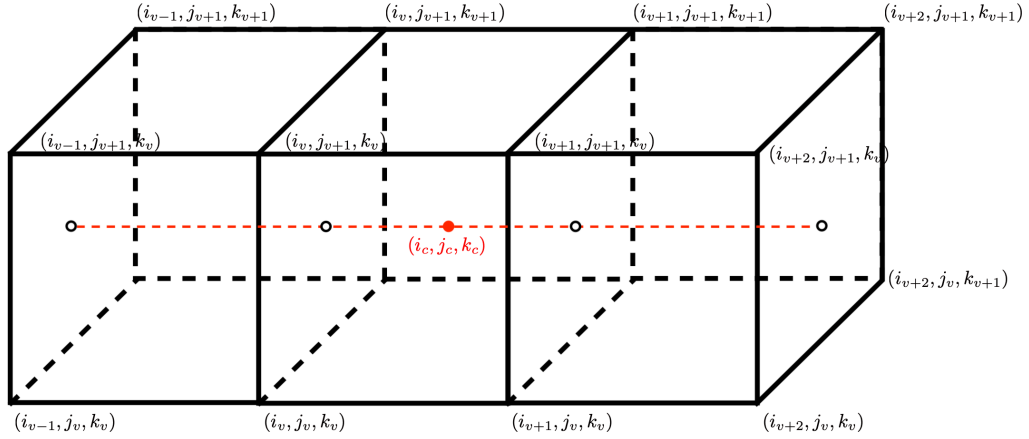


Figure 2: Computation of  $\partial_{xx}^c u_v(i_c, j_c, k_c)$ .

Assuming again that at every mesh vertex  $v(i_v, j_v, k_v)$  it holds that  $u_v(i_v, j_v, k_v) = u(x_v(i_v), y_v(j_v), z_v(k_v))$ , a straightforward Taylor expansion implies that

$$\begin{aligned} \left( \frac{\partial^2 u}{\partial x^2} \right)_c &= \partial_{xx}^c u_v(i_v, j_v, k_v) + \mathcal{O}(h^2), & \left( \frac{\partial^2 u}{\partial y^2} \right)_c &= \partial_{yy}^c u_v(i_v, j_v, k_v) + \mathcal{O}(h^2), \\ \left( \frac{\partial^2 u}{\partial z^2} \right)_c &= \partial_{zz}^c u_v(i_v, j_v, k_v) + \mathcal{O}(h^2), \end{aligned} \quad (13)$$

where again  $(\partial^2 u / \partial x^2)_c$ ,  $(\partial^2 u / \partial y^2)_c$ , and  $(\partial^2 u / \partial z^2)_c$  are the second derivatives of  $u$  computed at the center of cell  $c(i_c, j_c, k_c)$ . As reflected by the term  $\mathcal{O}(h^2)$  these formulas provide a second-order accurate approximation of the second derivatives of  $u$  along X, Y and Z. More details are reported in B.

Consider the discrete derivative along X given by (10) (the same argument applies to the other derivatives). We can apply this formula directly to  $u_v^{TT}(i_v, j_v, k_v)$  since we assume that the TT format representation of  $u_v$  is exact, i.e.,  $u_v^{TT}(i_v, j_v, k_v) = u_v(i_v, j_v, k_v)$ . As for the first derivatives, we must now see what this formula implies for the cores of  $u_v^{TT}$ . For  $i_v - 1 + m$  with  $m = 0, 1, 2, 3$ , by using the values of coefficients  $\xi_n, \xi_p = \pm 1$ , and expanding the double

internal summation we obtain:

$$\begin{aligned}
& \sum_{n=0}^1 \sum_{p=0}^1 \xi_n \xi_p u_v^{TT}(i_v - 1 + m, j_v + n, k_v + p) \\
&= u_v^{TT}(i_v - 1 + m, j_v, k_v) - u_v^{TT}(i_v - 1 + m, j_v + 1, k_v) - u_v^{TT}(i_v - 1 + m, j_v, k_v + 1) \\
&\quad + u_v^{TT}(i_v - 1 + m, j_v + 1, k_v + 1) \\
&= U_1(i_v - 1 + m)U_2(j_v)U_3(k_v) - U_1(i_v - 1 + m)U_2(j_v + 1)U_3(k_v) \\
&\quad - U_1(i_v - 1 + m)U_2(j_v)U_3(k_v + 1) + U_1(i_v - 1 + m)U_2(j_v + 1)U_3(k_v + 1) \\
&= U_1(i_v - 1 + m) \left( U_2(j_v) + U_2(j_v + 1) \right) \left( U_3(k_v) + U_3(k_v + 1) \right).
\end{aligned}$$

Then, expanding the first summation term in (10), using the values of coefficient  $\eta_m$  for  $m = 0, 1, 2, 3$ , and reordering the matrix slices  $U_1(i_v - 1 + m)$  for various  $m$ , we obtain:

$$\begin{aligned}
& \sum_{m=0}^3 \eta_m \sum_{n=0}^1 \sum_{p=0}^1 \xi_n \xi_p u_v^{TT}(i_v - 1 + m, j_v + n, k_v + p) \\
&= \left[ \sum_{m=0}^3 \eta_m U_1(i_v - 1 + m) \right] \left( U_2(j_v) + U_2(j_v + 1) \right) \left( U_3(k_v) + U_3(k_v + 1) \right) \\
&= \left[ \left( U_1(i_v + 2) - U_1(i_v + 1) \right) - \left( U_1(i_v) - U_1(i_v - 1) \right) \right] \left( U_2(j_v) + U_2(j_v + 1) \right) \left( U_3(k_v) + U_3(k_v + 1) \right).
\end{aligned}$$

Finally, we obtain the expression of the second discrete derivative of  $u_v^{TT}$ , which has the form:

$$\begin{aligned}
\partial_{xx}^c u_v^{TT}(i_c, j_c, k_c) &= U_1^{xx}(i_c) U_2^{xx}(j_c) U_3^{xx}(k_c) \\
&:= \frac{1}{2h_x} \left( \frac{U_1(i_v + 2) - U_1(i_v + 1)}{h_x} - \frac{U_1(i_v) - U_1(i_v - 1)}{h_x} \right) \left( \frac{U_2(j_v) + U_2(j_v + 1)}{2} \right) \times \\
&\quad \times \left( \frac{U_3(k_v) + U_3(k_v + 1)}{2} \right),
\end{aligned}$$

where, as for the first derivative, we associate the derivatives stencil  $\{(i_v - 1, i_v, i_v + 1, i_v + 2), (j_v, j_v + 1), (k_v, k_v + 1)\}$  with the cell indices  $i_c, j_c, k_c$ , and identify  $U_1^{xx}(i_c)$ ,  $U_2^{xx}(j_c)$  and  $U_3^{xx}(k_c)$ , the core matrices parametrized with the spatial indices  $i_c, j_c$ , and  $k_c$ , with the cores of the second derivative of  $u_v^{TT}(i_v, j_v, k_v)$ . Moreover, a comparison with the formulas for the first derivative shows that:

$$\partial_{xx}^c u_v^{TT}(i_c, j_c, k_c) = \frac{\partial_x^c u_v^{TT}(i_c + 1, j_c, k_c) - \partial_x^c u_v^{TT}(i_c - 1, j_c, k_c)}{2h_x}.$$

Similarly, we have the formulas for the other two second derivatives

$$\begin{aligned}
\partial_{yy}^c u_v^{TT}(i_c, j_c, k_c) &= U_1^{yy}(i_c) U_2^{yy}(j_c) U_3^{yy}(k_c) \\
&:= \frac{1}{2h_y} \left( \frac{U_1(i_v) + U_1(i_v + 1)}{2} \right) \left( \frac{U_2(j_v + 2) - U_2(j_v + 1)}{h_y} - \frac{U_2(j_v) - U_2(j_v - 1)}{h_y} \right) \times \\
&\quad \times \left( \frac{U_3(k_v) + U_3(k_v + 1)}{2} \right) \\
&= \frac{\partial_y^c u_v^{TT}(i_c, j_c + 1, k_c) - \partial_y^c u_v^{TT}(i_c, j_c - 1, k_c)}{2h_y},
\end{aligned}$$

and

$$\begin{aligned}
\partial_{zz}^c u_v^{TT}(i_c, j_c, k_c) &= U_1^{zz}(i_c) U_2^{zz}(j_c) U_3^{zz}(k_c) \\
&:= \frac{1}{2h_z} \left( \frac{U_1(i_v) + U_1(i_v + 1)}{2} \right) \left( \frac{U_2(j_v) + U_2(j_v + 1)}{2} \right) \times \\
&\quad \times \left( \frac{U_3(k_v + 2) - U_3(k_v + 1)}{h_z} - \frac{U_3(k_v) - U_3(k_v - 1)}{h_z} \right) \\
&= \frac{\partial_z^c u_v^{TT}(i_c, j_c, k_c + 1) - \partial_z^c u_v^{TT}(i_c, j_c, k_c - 1)}{2h_z}.
\end{aligned}$$

As for the first derivatives, a crucial point in this construction is that these operations do not introduce any additional error in the TT representation of the second derivatives other than those of the finite difference approximation. Although we will not use them in this work, for completeness' sake, we provide a possible discretization of the *mixed* second derivatives of the vertex grid function  $u_v$ :

$$\begin{aligned}
\partial_{xy}^c u_v^{TT}(i_c, j_c, k_c) &= \frac{1}{2} \left( \frac{\partial_x^c u_v^{TT}(i_c, j_c + 1, k_c) - \partial_x^c u_v^{TT}(i_c, j_c - 1, k_c)}{2h_y} \right. \\
&\quad \left. + \frac{\partial_y^c u_v^{TT}(i_c + 1, j_c, k_c) - \partial_y^c u_v^{TT}(i_c - 1, j_c, k_c)}{2h_x} \right), \\
\partial_{yz}^c u_v^{TT}(i_c, j_c, k_c) &= \frac{1}{2} \left( \frac{\partial_y^c u_v^{TT}(i_c, j_c, k_c + 1) - \partial_y^c u_v^{TT}(i_c, j_c, k_c - 1)}{2h_z} \right. \\
&\quad \left. + \frac{\partial_z^c u_v^{TT}(i_c, j_c + 1, k_c) - \partial_z^c u_v^{TT}(i_c, j_c - 1, k_c)}{2h_y} \right), \\
\partial_{zx}^c u_v^{TT}(i_c, j_c, k_c) &= \frac{1}{2} \left( \frac{\partial_z^c u_v^{TT}(i_c + 1, j_c, k_c) - \partial_z^c u_v^{TT}(i_c - 1, j_c, k_c)}{2h_x} \right. \\
&\quad \left. + \frac{\partial_x^c u_v^{TT}(i_c, j_c, k_c + 1) - \partial_x^c u_v^{TT}(i_c, j_c, k_c - 1)}{2h_z} \right).
\end{aligned}$$

A straightforward calculation shows that the first formula is symmetric by swapping  $x$  and  $y$ , i.e., thus formally giving  $\partial_{xy}^c u_v^{TT}(i_c, j_c, k_c) = \partial_{yx}^c u_v^{TT}(i_c, j_c, k_c)$ ; the second one by swapping  $y$  and  $z$ , thus formally giving  $\partial_{yz}^c u_v^{TT}(i_c, j_c, k_c) = \partial_{zy}^c u_v^{TT}(i_c, j_c, k_c)$ , and the third one by swapping  $z$  and  $x$ , thus formally giving  $\partial_{zx}^c u_v^{TT}(i_c, j_c, k_c) = \partial_{xz}^c u_v^{TT}(i_c, j_c, k_c)$ . The efficient implementation must be performed at the core level, thus leading to formulas similar to the ones for  $\partial_{xx}^c u_v^{TT}$ ,  $\partial_{yy}^c u_v^{TT}$ , and  $\partial_{zz}^c u_v^{TT}$ . However, the average will change the internal ranks and a rounding step could be necessary.

**Remark 3.1.** The alternative formulas that define the discrete second derivatives in TT format as the difference between the discrete first derivatives in TT format have an obvious correspondence in the full-grid formulation, as we can write, for example, that

$$\partial_{xx}^c u_v(i_c, j_c, k_c) = \frac{\partial_x^c u_v(i_c + 1, j_c, k_c) - \partial_x^c u_v(i_c - 1, j_c, k_c)}{2h_x}.$$

Similar difference formulas hold for all the other discrete second derivatives. Moreover, they provide an alternative way to implement the calculation of the second derivatives, which is useful in the next extension of this approach to the case of meshes obtained from non-equispaced univariate partitions in X, Y and Z and regular equispaced meshes partitioning remapped domains.

### 3.4 Discrete Laplacian of vertex grid functions

Summing the discrete second derivatives of the vertex grid function  $u_v$  naturally yields the discrete Laplacian

$$\Delta^c u_v(i_c, j_c, k_c) = \partial_{xx}^c u_v(i_c, j_c, k_c) + \partial_{yy}^c u_v(i_c, j_c, k_c) + \partial_{zz}^c u_v(i_c, j_c, k_c).$$

Hereafter, we will refer to the cell grid function  $\Delta^c u_v$  as the *discrete cell Laplacian* of the vertex grid function  $u_v$ .

Since we seek for an approximation of  $u$  at the mesh vertices, we interpolate  $\Delta^c u_v$  at the grid vertices  $v(i_v, j_v, k_v)$  to obtain the vertex grid function  $\Delta^v u_v$ , i.e., the *discrete vertex laplacian* of the grid function  $u_v$ . Formally, we introduce a vertex interpolation operator, denoted by  $\mathcal{I}^v$ , such that

$$\Delta^v u_v = \mathcal{I}^v(\Delta^c u_v),$$

or, locally, that

$$\Delta^v u_v(i_v, j_v, k_v) = \mathcal{I}_{i_v, j_v, k_v}^v(\Delta^c u_v).$$

On a regular mesh where all first neighbor cell-centers around a given vertex are equidistant from that vertex, and the interpolation is nothing but the arithmetic average:

$$\mathcal{I}_{i_v, j_v, k_v}^v(\Delta^c u_v)(i_v, j_v, k_v) = \frac{1}{8} \sum_{m, n, p=0}^1 (\Delta^c u_v)(i_c + m, j_c + n, k_c + p).$$

The same definitions hold for  $u_v^{TT}$ , the tensor-train representation of  $u_v$ , so that the *discrete cell Laplacian in TT format* reads as

$$\Delta^{c, TT} u_v^{TT}(i_c, j_c, k_c) = \text{rndg}(\partial_{xx}^c u_v^{TT}(i_c, j_c, k_c) + \partial_{yy}^c u_v^{TT}(i_c, j_c, k_c) + \partial_{zz}^c u_v^{TT}(i_c, j_c, k_c)),$$

where we recall that  $\text{rndg}(\cdot)$  is the rounding operator that we discussed at the end of Section 2. The *discrete vertex Laplacian in TT format* reads as

$$\Delta^{v, TT} u_v^{TT} = \mathcal{I}^{v, TT}(\Delta^{c, TT} u_v^{TT}),$$

or, locally, as

$$\Delta^{v, TT} u_v^{TT}(i_v, j_v, k_v) = \mathcal{I}_{i_v, j_v, k_v}^{v, TT}(\Delta^{c, TT} u_v^{TT}).$$

The vertex interpolation is still the arithmetic average and can be implemented very efficiently, working directly on the cores of tensor  $\Delta^{c, TT} u_v^{TT}(i_c, j_c, k_c)$ :

$$\begin{aligned} \mathcal{I}_{i_v, j_v, k_v}^v(\Delta^{c, TT} u_v^{TT})(i_v, j_v, k_v) &= \frac{1}{8} \sum_{m, n, p=0}^1 (\Delta^{c, TT} u_v^{TT})(i_c + m, j_c + n, k_c + p) \\ &= \left( \frac{U_1^{xx}(i_c) + U_1^{xx}(i_c + 1)}{2} \right) \left( \frac{U_2^{yy}(j_c) + U_2^{yy}(j_c + 1)}{2} \right) \left( \frac{U_3^{zz}(k_c) + U_3^{zz}(k_c + 1)}{2} \right). \end{aligned}$$

Such average operation does not change the TT ranks of  $\Delta^{c, TT} u_v^{TT}$ , so no additional rounding needs to be performed.

### 3.5 Boundary conditions

We manage the boundary conditions by using boundary layers of ghost cells. In particular, we assume that there are  $N^{\text{bnd}}$  external frames of cells, which requires  $N^{\text{bnd}} + 1$  layers of boundary vertices, surrounding the hyper-rectangular domain ( $N^{\text{bnd}} = 2$  in this work). These frames correspond to the set of vertex indices:

- faces orthogonal to X:  $0 \leq i_v \leq N^{\text{bnd}}$  and  $N_v^x - 1 - N^{\text{bnd}} \leq i_v \leq N_v^x - 1$  for all values of  $j_v$  and  $k_v$ ;
- faces orthogonal to Y:  $0 \leq j_v \leq N^{\text{bnd}}$  and  $N_v^y - 1 - N^{\text{bnd}} \leq j_v \leq N_v^y - 1$  for all values of  $i_v$  and  $k_v$ ;
- faces orthogonal to Z:  $0 \leq k_v \leq N^{\text{bnd}}$  and  $N_v^z - 1 - N^{\text{bnd}} \leq k_v \leq N_v^z - 1$  for all values of  $k_v$  and  $i_v$ ,

and to the set of cell indices:

- faces orthogonal to X:  $0 \leq i_c < N^{\text{bnd}}$  and  $N_c^x - 1 - N^{\text{bnd}} \leq i_c < N_c^x - 1$  for all values of  $j_c$  and  $k_c$ ;

- faces orthogonal to Y:  $0 \leq j_c < N_c^{\text{bnd}}$  and  $N_c^y - 1 - N_c^{\text{bnd}} \leq j_c < N_c^y - 1$  for all values of  $i_c$  and  $k_c$ ;
- faces orthogonal to Z:  $0 \leq k_c < N_c^{\text{bnd}}$  and  $N_c^z - 1 - N_c^{\text{bnd}} \leq k_c < N_c^z - 1$  for all values of  $i_c$  and  $j_c$ .

Setting Dirichlet boundary conditions in the full-grid implementation is straightforward, basically consisting in a loop over all ghost vertices and cell centers, where the values of the exact solution is computed and then assigned to  $u_v$ . Setting Dirichlet boundary conditions on the TT representations of  $u_v$  is different and a bit trickier since the vertex values of  $u_v^{TT}$  are not stored in the computer memory and are accessible only in an indirect way. To enforce such boundary conditions, we modify the TT cores directly, following the approach of [24]. The process involves three steps, illustrated in Figure 3:

- setting to zero the first and last  $N^{\text{bnd}}$  slices of the  $u_v^{TT}$  core, corresponding to the boundary vertices;
- building a new tensor  $\mathcal{B}$  whose values at the internal indices are zero and whose boundary slices in the cores of  $u_v^{TT}$  corresponding to the boundary vertices match a decomposition of the boundary data;
- replacing  $u_v^{TT}$  with the sum  $u_v^{TT} + \mathcal{B}$ .

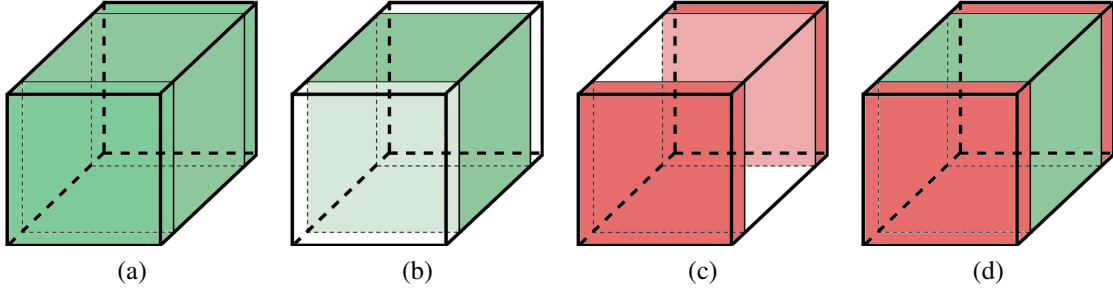


Figure 3: Setting of the boundary conditions along one direction: (a) original tensor  $u_v^{TT}$ ; (b)  $u_v^{TT}$  with first and last slices set to zero; (c) tensor  $\mathcal{B}$  with zero inside and exact values on the first and last slices; (d) final tensor  $u_v^{TT} + \mathcal{B}$ .

The boundary slices can be built directly if the boundary condition functions are already in a separated variable form, or can be obtained by performing a dyadic decomposition, for example, by using the SVD. If the number of dimensions is bigger than three, the boundary slices can be obtained by the TT-SVD algorithm [29] or the cross-interpolation algorithm [30].

## 4 Extensions to variable-sized grids and remapped domains

In this section, we extend the finite difference/finite volume discretization framework of the previous section to handle more general computational domains. Specifically, we consider two important generalizations: non-uniform grid spacing with variable-sized cells and domains that can be remapped onto a cubic domain through orthogonal coordinate transformations. These extensions allow our numerical methods to be applied to a broader class of problems while maintaining the advantageous properties of the tensor-train format.

### 4.1 Full-grid and tensor-train discretizations on variable-sized grids

Assume that the three univariate partitions  $\{x(i_v), i_v = 0, 1, \dots, N_v^x - 1\}$ ,  $\{y(j_v), j_v = 0, 1, \dots, N_v^y - 1\}$ , and  $\{z(k_v), k_v = 0, 1, \dots, N_v^z - 1\}$  along, respectively, X, Y and Z, have non-constant step sizes  $h_{x,i_c} = x(i_v + 1) - x(i_v)$ ,  $h_{y,j_c} = y(j_v + 1) - y(j_v)$ , and  $h_{z,k_c} = z(k_v + 1) - z(k_v)$ . The resulting mesh will be an orthogonal grid with a non-uniform grid spacing, as the one presented in Figure 4. This type of computational mesh is useful in applications requiring more accuracy near a domain boundary, for example, in the case the problem solution presents a boundary layer with a sharp gradient at that boundary.

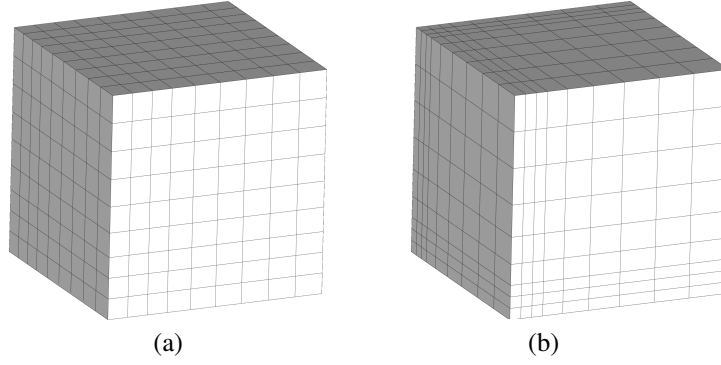


Figure 4: Variable-sized grids with geometrically varying step sizes  $h_{x,i_c} = r_X h_{x,i_c-1}$ ,  $h_{y,j_c} = r_Y h_{y,j_c-1}$ ,  $h_{z,k_c} = r_Z h_{z,k_c-1}$  and uniform step size ratios: (a)  $r_X = r_Y = r_Z = 1.125$ ; (b)  $r_X = r_Y = r_Z = 1.5$

To obtain the formulas defining the discrete gradient components of a vertex grid function  $u_v$ , i.e.,  $(\partial_x^c u_v, \partial_y^c u_v, \partial_z^c u_v)$  and their TT representations  $(\partial_x^c u_v^{TT}, \partial_y^c u_v^{TT}, \partial_z^c u_v^{TT})$ , we need to use the variable step sizes  $h_{x,i_v}$ ,  $h_{y,j_v}$ , and  $h_{z,k_v}$  consistently. With a simple modification, the discrete first derivatives along X are now given by:

$$\partial_x^c u_v(i_c, j_c, k_c) = \frac{1}{4h_{x,i_c}} \sum_{n=0}^1 \sum_{p=0}^1 \left( u_v(i_v + 1, j_v + n, k_v + p) - u_v(i_v, j_v + n, k_v + p) \right),$$

$$\partial_x^c u_v^{TT}(i_c, j_c, k_c) = \left( \frac{U_1(i_v + 1) - U_1(i_v)}{h_{x,i_c}} \right) \left( \frac{U_2(j_v) + U_2(j_v + 1)}{2} \right) \left( \frac{U_3(k_v) + U_3(k_v + 1)}{2} \right),$$

and the formulas for  $\partial_y^c u_v$ ,  $\partial_z^c u_v$ ,  $\partial_y^c u_v^{TT}$ , and  $\partial_z^c u_v^{TT}$  are obtained accordingly. The second derivatives are defined similarly. First, we add and subtract  $\partial_x^c u_v(i_c, j_c, k_c)$  to the difference between the discrete first derivative of  $u_v$  at cells  $(i_c + 1, j_c, k_c)$  and  $(i_c - 1, j_c, k_c)$ :

$$\partial_x^c u_v(i_c + 1, j_c, k_c) - \partial_x^c u_v(i_c - 1, j_c, k_c) = [\partial_x^c u_v(i_c + 1, j_c, k_c) - \partial_x^c u_v(i_c, j_c, k_c)] + [\partial_x^c u_v(i_c, j_c, k_c) - \partial_x^c u_v(i_c - 1, j_c, k_c)].$$

Then, we subdivide the first difference by  $h_{x,i_c+1}$  and the second by  $h_{x,i_c}$  and we take the arithmetic average; we find that

$$\partial_{xx}^c u_v(i_c, j_c, k_c) = \frac{1}{2} \frac{\partial_x^c u_v(i_c + 1, j_c, k_c) - \partial_x^c u_v(i_c, j_c, k_c)}{h_{x,i_c+1}} + \frac{1}{2} \frac{\partial_x^c u_v(i_c, j_c, k_c) - \partial_x^c u_v(i_c - 1, j_c, k_c)}{h_{x,i_c}}.$$

By repeating the same construction, we find the second derivatives along the other directions:

$$\partial_{yy}^c u_v(i_c, j_c, k_c) = \frac{1}{2} \frac{\partial_y^c u_v(i_c, j_c + 1, k_c) - \partial_y^c u_v(i_c, j_c, k_c)}{h_{y,j_c+1}} + \frac{1}{2} \frac{\partial_y^c u_v(i_c, j_c, k_c) - \partial_y^c u_v(i_c, j_c - 1, k_c)}{h_{y,j_c}},$$

$$\partial_{zz}^c u_v(i_c, j_c, k_c) = \frac{1}{2} \frac{\partial_z^c u_v(i_c, j_c, k_c + 1) - \partial_z^c u_v(i_c, j_c, k_c)}{h_{z,k_c+1}} + \frac{1}{2} \frac{\partial_z^c u_v(i_c, j_c, k_c) - \partial_z^c u_v(i_c, j_c, k_c - 1)}{h_{z,k_c}},$$

and in the TT format:

$$\partial_{xx}^c u_v^{TT}(i_c, j_c, k_c) = \frac{1}{2} \frac{\partial_x^c u_v^{TT}(i_c + 1, j_c, k_c) - \partial_x^c u_v^{TT}(i_c, j_c, k_c)}{h_{x,i_c+1}} + \frac{1}{2} \frac{\partial_x^c u_v^{TT}(i_c, j_c, k_c) - \partial_x^c u_v^{TT}(i_c - 1, j_c, k_c)}{h_{x,i_c}},$$

$$\partial_{yy}^c u_v^{TT}(i_c, j_c, k_c) = \frac{1}{2} \frac{\partial_y^c u_v^{TT}(i_c, j_c + 1, k_c) - \partial_y^c u_v^{TT}(i_c, j_c, k_c)}{h_{y,j_c+1}} + \frac{1}{2} \frac{\partial_y^c u_v^{TT}(i_c, j_c, k_c) - \partial_y^c u_v^{TT}(i_c, j_c - 1, k_c)}{h_{y,j_c}},$$

$$\partial_{zz}^c u_v^{TT}(i_c, j_c, k_c) = \frac{1}{2} \frac{\partial_z^c u_v^{TT}(i_c, j_c, k_c + 1) - \partial_z^c u_v^{TT}(i_c, j_c, k_c)}{h_{z,k_c+1}} + \frac{1}{2} \frac{\partial_z^c u_v^{TT}(i_c, j_c, k_c) - \partial_z^c u_v^{TT}(i_c, j_c, k_c - 1)}{h_{z,k_c}}.$$

The vertex interpolation algorithm has to be modified accordingly. For simplicity, we consider the 1D case where we interpolate cell-centered quantities like  $\{u_c(i_c)\}$  that are defined at the cell centers  $x_c(i_c)$  to the vertex-centered quantity  $u_v(i_v)$  at vertex positions  $x_v(i_v)$ . The interpolated value  $u_v(i_v)$  is the weighted average on the stencil  $\{i_c - 1, i_c\}$ :

$$u_v(i_v) = \frac{u_c(i_c - 1)\Delta x_{i_c - 1} + u_c(i_c)\Delta x_{i_c}}{\Delta x_{i_c - 1} + \Delta x_{i_c}}, \quad (14)$$

where  $\Delta x_{i_c - 1} = x_v(i_v) - x_c(i_c - 1)$  is the distance between vertex  $i_v$  and the left cell center, and  $\Delta x_{i_c} = x_c(i_c) - x_v(i_v)$  is the distance between vertex  $i_v$  and the right cell center. The vertex interpolation in 3D is done by applying the 1D vertex interpolation dimension by dimension. For a vertex grid tensor in TT format, we apply the 1D interpolation independently to each TT core, the resulting multi-dimensional interpolation being expressed as a tensor product of the 1D interpolations.

The construction of the Laplace operator and the setting of the boundary conditions then continues as in Sections 3.4-3.5.

## 4.2 Full-grid and tensor-train discretizations on remapped domains

In the previous sections, we discussed the finite difference discretization of first and second derivatives in a full-grid and tensor-train format using orthogonal, Cartesian meshes that are obtained by a tensor product of univariate partitions along the coordinate axis X, Y, and Z. In this section, we generalize the grid partitions to the case of hyper-rectangular 3D domains remapped onto a cube, see Figure 5. In particular, we assume that the remapping functions are also univariate so that the resulting multiplicative coefficients do not affect the rank of the tensor-train finite difference formulas.

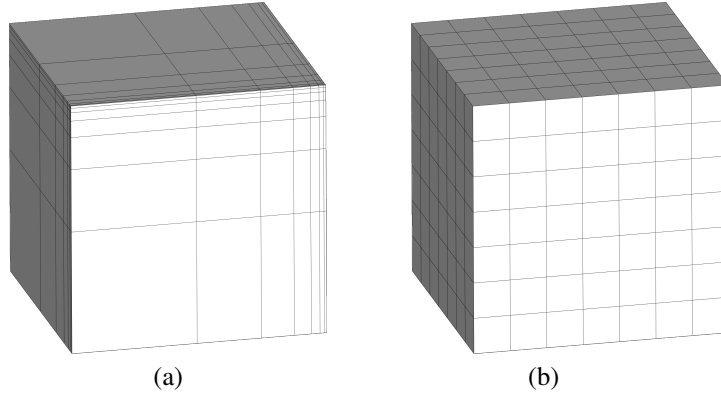


Figure 5: Hyper-rectangular 3D domain  $\Omega$  (a) and its remapping onto a cube  $\tilde{\Omega}$  (b).

Consider the Laplace operator of the function  $\tilde{u} : \tilde{\Omega} \rightarrow \mathbb{R}$  with respect to the coordinate framework  $(\tilde{x}, \tilde{y}, \tilde{z})$  defined as:

$$\tilde{\Delta}\tilde{u} = \frac{\partial^2 \tilde{u}}{\partial \tilde{x}^2} + \frac{\partial^2 \tilde{u}}{\partial \tilde{y}^2} + \frac{\partial^2 \tilde{u}}{\partial \tilde{z}^2}.$$

We establish a mapping between the domains  $\Omega$  and  $\tilde{\Omega}$  through three independent, nonsingular, smooth coordinate transformations

$$\begin{cases} x = x(\tilde{x}), \\ y = y(\tilde{y}), \\ z = z(\tilde{z}), \end{cases} \quad \text{and their inverse transformations} \quad \begin{cases} \tilde{x} = \tilde{x}(x), \\ \tilde{y} = \tilde{y}(y), \\ \tilde{z} = \tilde{z}(z). \end{cases} \quad (15)$$

Consider the function  $u : \Omega \rightarrow \mathbb{R}$  that corresponds to the function  $\tilde{u}$  defined on  $\tilde{\Omega}$  through the coordinate map

introduced above so that  $u(x, y, z) = \tilde{u}(\tilde{x}(x), \tilde{y}(y), \tilde{z}(z))$ . Its Laplace operator is given by:

$$\begin{aligned} \Delta u = & \left( \frac{\partial \tilde{x}(x)}{\partial x} \right)^{-1} \frac{\partial}{\partial x} \left[ \left( \frac{\partial \tilde{x}(x)}{\partial x} \right)^{-1} \frac{\partial u}{\partial x} \right] + \left( \frac{\partial \tilde{y}(y)}{\partial y} \right)^{-1} \frac{\partial}{\partial y} \left[ \left( \frac{\partial \tilde{y}(y)}{\partial y} \right)^{-1} \frac{\partial u}{\partial y} \right] + \\ & + \left( \frac{\partial \tilde{z}(z)}{\partial z} \right)^{-1} \frac{\partial}{\partial z} \left[ \left( \frac{\partial \tilde{z}(z)}{\partial z} \right)^{-1} \frac{\partial u}{\partial z} \right]. \end{aligned} \quad (16)$$

The construction of discrete derivatives proceeds in the same way as for variable-sized grids. Since the heat equation can be discretized on the remapped domain by using a regular, equispaced, orthogonal Cartesian grid, we assume  $h_x$ ,  $h_y$  and  $h_z$  to be constant. However, we must take into account the derivatives of the maps  $\tilde{x}(x)$ ,  $\tilde{y}(y)$ , and  $\tilde{z}(z)$  that appear in the remapped equations. We obtain the formulas defining the discrete gradient components of a vertex grid functions  $u_v$ , i.e.,  $(\partial_x^c u_v, \partial_y^c u_v, \partial_z^c u_v)$  and its TT representation  $(\partial_x^c u_v^{TT}, \partial_y^c u_v^{TT}, \partial_z^c u_v^{TT})$ , by consistently multiplying the step sizes  $h_x$ ,  $h_y$  and  $h_z$  by  $\tilde{x}'(i_c) = \partial \tilde{x}(x_c(i_c))/\partial x$ ,  $\tilde{y}'(j_c) = \partial \tilde{y}(y_c(j_c))/\partial y$ , and  $\tilde{z}'(k_c) = \partial \tilde{z}(z_c(k_c))/\partial z$ . Therefore, the discrete first derivatives along X, Y and Z are given by:

$$\begin{aligned} \partial_x^c u_v(i_c, j_c, k_c) &= \frac{1}{4\tilde{x}'(x_c(i_c))h_x} \sum_{n=0}^1 \sum_{p=0}^1 \left( u_v(i_v + 1, j_v + n, k_v + p) - u_v(i_v, j_v + n, k_v + p) \right) \\ \partial_y^c u_v(i_c, j_c, k_c) &= \frac{1}{4\tilde{y}'(y_c(j_c))h_y} \sum_{m=0}^1 \sum_{p=0}^1 \left( u_v(i_v + m, j_v + 1, k_v + p) - u_v(i_v + m, j_v, k_v + p) \right), \\ \partial_z^c u_v(i_c, j_c, k_c) &= \frac{1}{4\tilde{z}'(z_c(k_c))h_z} \sum_{m=0}^1 \sum_{n=0}^1 \left( u_v(i_v + m, j_v + n, k_v + 1) - u_v(i_v + m, j_v + n, k_v) \right), \end{aligned}$$

and their TT version are

$$\begin{aligned} \partial_x^c u_v^{TT}(i_c, j_c, k_c) &= \left( \frac{U_1(i_v + 1) - U_1(i_v)}{\tilde{x}'(x_c(i_c))h_x} \right) \left( \frac{U_2(j_v) + U_2(j_v + 1)}{2} \right) \left( \frac{U_3(k_v) + U_3(k_v + 1)}{2} \right), \\ \partial_y^c u_v^{TT}(i_c, j_c, k_c) &= \left( \frac{U_1(i_v) + U_1(i_v + 1)}{2} \right) \left( \frac{U_2(j_v + 1) - U_2(j_v)}{\tilde{y}'(y_c(j_c))h_y} \right) \left( \frac{U_3(k_v) + U_3(k_v + 1)}{2} \right), \\ \partial_z^c u_v^{TT}(i_c, j_c, k_c) &= \left( \frac{U_1(i_v) + U_1(i_v + 1)}{2} \right) \left( \frac{U_2(j_v) + U_2(j_v + 1)}{2} \right) \left( \frac{U_3(k_v + 1) - U_3(k_v)}{\tilde{z}'(z_c(k_c))h_z} \right). \end{aligned}$$

The second derivatives are obtained by repeating the same derivation as for variable-sized grids, still taking into account that now each mesh size is a constant value over the mesh but multiplied by a variable function from the remapping process. We obtain:

$$\begin{aligned} \partial_{xx}^c u_v(i_c, j_c, k_c) &= \frac{1}{2} \frac{\partial_x^c u_v(i_c + 1, j_c, k_c) - \partial_x^c u_v(i_c, j_c, k_c)}{\tilde{x}'(x_c(i_c + 1))h_x} + \frac{1}{2} \frac{\partial_x^c u_v(i_c, j_c, k_c) - \partial_x^c u_v(i_c - 1, j_c, k_c)}{\tilde{x}'(x_c(i_c))h_x}, \\ \partial_{yy}^c u_v(i_c, j_c, k_c) &= \frac{1}{2} \frac{\partial_y^c u_v(i_c, j_c + 1, k_c) - \partial_y^c u_v(i_c, j_c, k_c)}{\tilde{y}'(y_c(j_c + 1))h_y} + \frac{1}{2} \frac{\partial_y^c u_v(i_c, j_c, k_c) - \partial_y^c u_v(i_c, j_c - 1, k_c)}{\tilde{y}'(y_c(j_c))h_y}, \\ \partial_{zz}^c u_v(i_c, j_c, k_c) &= \frac{1}{2} \frac{\partial_z^c u_v(i_c, j_c, k_c + 1) - \partial_z^c u_v(i_c, j_c, k_c)}{\tilde{z}'(z_c(k_c + 1))h_z} + \frac{1}{2} \frac{\partial_z^c u_v(i_c, j_c, k_c) - \partial_z^c u_v(i_c, j_c, k_c - 1)}{\tilde{z}'(z_c(k_c))h_z}, \end{aligned}$$



and in the TT format:

$$\begin{aligned}\partial_{xx}^c u_v^{TT}(i_c, j_c, k_c) &= \frac{1}{2} \frac{\partial_x^c u_v^{TT}(i_c + 1, j_c, k_c) - \partial_x^c u_v^{TT}(i_c, j_c, k_c)}{\tilde{x}'(x_c(i_c + 1))h_x} + \frac{1}{2} \frac{\partial_x^c u_v^{TT}(i_c, j_c, k_c) - \partial_x^c u_v^{TT}(i_c - 1, j_c, k_c)}{\tilde{x}'(x_c(i_c))h_x}, \\ \partial_{yy}^c u_v^{TT}(i_c, j_c, k_c) &= \frac{1}{2} \frac{\partial_y^c u_v^{TT}(i_c, j_c + 1, k_c) - \partial_y^c u_v^{TT}(i_c, j_c, k_c)}{\tilde{y}'(y_c(j_c + 1))h_y} + \frac{1}{2} \frac{\partial_y^c u_v^{TT}(i_c, j_c, k_c) - \partial_y^c u_v^{TT}(i_c, j_c - 1, k_c)}{\tilde{y}'(y_c(j_c))h_y}, \\ \partial_{zz}^c u_v^{TT}(i_c, j_c, k_c) &= \frac{1}{2} \frac{\partial_z^c u_v^{TT}(i_c, j_c, k_c + 1) - \partial_z^c u_v^{TT}(i_c, j_c, k_c)}{\tilde{z}'(z_c(k_c + 1))h_z} + \frac{1}{2} \frac{\partial_z^c u_v^{TT}(i_c, j_c, k_c) - \partial_z^c u_v^{TT}(i_c, j_c, k_c - 1)}{\tilde{z}'(z_c(k_c))h_z}.\end{aligned}$$

The vertex interpolation is done by applying the same algorithm of (14) as for the case of variable size grids, the only difference being in the definition of the interpolation coefficients:

- $\Delta x_{i_c-1} = (\tilde{x}'(x_v(i_v)) - \tilde{x}'(x_c(i_c - 1)))h_x$  is the distance between vertex  $v(i_v)$  and the center of  $c(i_c - 1)$ , the cell on the left;
- $\Delta x_{i_c} = (\tilde{x}'(x_c(i_c)) - \tilde{x}'(x_v(i_v)))h_x$  is the distance between vertex  $v(i_v)$  and the center of  $c(i_c)$ , the cell on the right.

The construction of the Laplace operator and the setting of the boundary conditions then continue as in Sections 3.4-3.5.

**Remark 4.1.** The variable-sized grids of Section 4.1 can be expressed through a similar remapping algorithm when the vertex positions are determined by a set of remapping functions as in (15). In such a case, the numerical treatment is the same. However, the case considered in Section 4.1 is more general as it does not require an explicit knowledge of such remapping functions. This situation occurs, for example, when the mesh vertices are adaptively relocated in the domain according to an a-posteriori error indicator.

## 5 Time integration

We partition the time interval  $[0, T]$  using a time step with constant size  $\Delta t$ , and denote the intermediate time instants as  $t^n = n\Delta t$  for  $n = 0, 1, \dots, N_{\Delta t}$ , where  $N_{\Delta t} = T/\Delta t$  is the total number of time steps. Let  $u_v^n$  and  $u_v^{TT,n}$  be the time discretizations  $u_v(\cdot; t^n)$  and  $u_v^{TT}(\cdot; t^n)$ , the full-grid and tensor-train vertex grid functions that approximate  $u(\cdot, t)$  at  $t = t^n$ . We discretize the time derivatives of  $u_v(\cdot; t)$  and  $u_v^{TT}(\cdot; t)$  using the first-order accurate in time finite difference formula, so that  $(\partial u_v / \partial t)^n \approx (u_v^{n+1} - u_v^n) / \Delta t$  and  $(\partial u_v^{TT} / \partial t)^n \approx (u_v^{TT,n+1} - u_v^{TT,n}) / \Delta t$ .

To update  $u_v^n$  to  $u_v^{n+1}$  and  $u_v^{TT,n}$  to  $u_v^{TT,n+1}$ , we consider three different integration schemes: the explicit Euler scheme, the implicit Euler scheme, and the semi-implicit Crank-Nicolson scheme. The explicit Euler scheme, while straightforward to implement, is only first-order accurate in time, and its simplicity comes at the cost of a potential instability that may require smaller time steps. It is worth noting that the explicit and implicit Euler schemes are also building blocks of higher-order algorithms, e.g., the Runge-Kutta scheme, with improved accuracy and bigger storage and computational costs. In our formulation, we adopt a similar strategy and split the Crank-Nicolson scheme in two steps with an initial explicit step followed by an implicit one, both advancing the numerical solution of  $\Delta t/2$ .

Let  $f_v^{n+\theta}$ ,  $\theta \in \{0, 1/2, 1\}$ , denote the source term evaluated at the time  $t^n + \theta\Delta t$  at the mesh vertices. The TT reformulation requires a TT decomposition of this term, which can be performed using a tensor-train decomposition algorithm such as the TT-SVD or the *cross-interpolation algorithm*, see, e.g., [29, 30], and the comment at the end of Section 2. We let  $f_v^{TT}(\cdot; t)$  denote the tensor-train representation of the vertex grid function  $f_v(\cdot; t)$  that is obtained by sampling the forcing function  $f(\cdot, t)$  at time  $t$  at the mesh vertices. For  $\theta = 1/2$ , as in the Crank-Nicolson scheme, we use the approximation  $f^{n+1/2} \approx (f^n + f^{n+1})/2$ , which is still second-order accurate and does not affect the global accuracy of our method.

Hereafter, we will refer to the vertex grid functions  $\Delta t(\Delta^v u_v + f_v)$  and the corresponding tensor-train representation  $\Delta t(\Delta^{v,TT} u_v^{TT} + f_v^{TT})$  as the *vertex residual terms* or, simply, *residual term*. Finally, we note that the construction of both  $\Delta^v u_v$  and  $\Delta^{v,TT} u_v^{TT}$  already takes into account the Dirichlet boundary conditions, which are explicitly set in the ghost vertex and cell frames at the same time instant at which we consider the fields  $u_v$  and  $u_v^{TT}$ . Therefore, we only perform the update of  $u_v$  and  $u_v^{TT}$  at the internal vertices.

**Explicit Euler scheme** The explicit Euler scheme evaluates the residual term at the time  $t^n$ , so that

$$u_v^{n+1} = u_v^n + \Delta t (\Delta^v u_v^n + f_v^n). \quad (17)$$

In the TT reformulation, we first perform a similar update:

$$\bar{u}_v^{TT,n+1} = u_v^{TT,n} + \Delta t (\Delta^{v,TT} u_v^{TT,n} + f_v^{TT,n}), \quad (18)$$

again for all index triple  $(i_v, j_v, k_v)$  corresponding to the *internal* vertices, and then we apply the rounding algorithm

$$u_v^{TT,n+1} = \text{rndg}(\bar{u}_v^{TT,n+1}). \quad (19)$$

Algorithm 2 in D provides implementation details on the update from  $u_v^{TT,n}$  to  $u_v^{TT,n+1}$ .

**Implicit Euler scheme** The implicit Euler method evaluates the residual term at the time  $t^{n+1}$ , so that

$$u_v^{n+1} - \Delta t \Delta^v u_v^{n+1} = u_v^n + \Delta t f_v^{n+1}. \quad (20)$$

In the TT reformulation, we perform a similar update:

$$u_v^{TT,n+1} - \Delta t \Delta^{v,TT} u_v^{TT,n+1} = u_v^{TT,n} + \Delta t f_v^{TT,n+1}. \quad (21)$$

Both formulations (20) and (21) require the resolution of a linear system that we iteratively solve by applying a *matrix-free Preconditioned Conjugate Gradient (PCG) method*. Krylov methods need to perform the *matrix-vector multiplication* of the coefficient matrix times the current conjugate direction at every iteration. In the matrix-free setting, we perform this by evaluating the left-hand side of (20) and (21) on the conjugate direction fields. The details of the implementation and the design of a preconditioner that is suitable to the TT formulation are discussed in the next subsection. Algorithm 3 in D provides implementation details on the update from  $u_v^{TT,n}$  to  $u_v^{TT,n+1}$ , including the rounding procedure that is performed inside the PCG to control the rank growth.

**Semi-implicit Crank-Nicolson scheme** The semi-implicit Crank-Nicolson scheme evaluates the residual term at the half-time step  $t^{n+1/2} = t + \Delta t/2$ . We approximate this evaluation by taking the average of the residual at the initial and final times, i.e.,  $t^n$  and  $t^{n+1}$  so that the time marching schemes read as:

$$u_v^{n+1} - \frac{\Delta t}{2} (\Delta^v u_v^{n+1} + f_v^{n+1}) = u_v^n + \frac{\Delta t}{2} (\Delta^v u_v^n + f_v^n),$$

and

$$u_v^{TT,n+1} - \frac{\Delta t}{2} (\Delta^{v,TT} u_v^{TT,n+1} + f_v^{TT,n+1}) = u_v^{TT,n} + \frac{\Delta t}{2} (\Delta^{v,TT} u_v^{TT,n} + f_v^{TT,n}).$$

This approach allows us to split the time step into two consecutive half steps. The first step uses the explicit Euler scheme to advance the solution from  $u_v^n$  (or  $u_v^{TT,n}$ ) to an intermediate solution  $u_v^{n+1/2}$  (or  $u_v^{TT,n+1/2}$ ) at time  $t^{n+1/2} = t^n + \Delta t/2$ . The second step uses the implicit Euler scheme to advance the intermediate solution from  $u_v^{n+1/2}$  (or  $u_v^{TT,n+1/2}$ ) to the final time step  $u_v^{n+1}$  (or  $u_v^{TT,n+1}$ ). We can thus reformulate the Crank-Nicolson scheme as follows:

(1) *Explicit step*: use formula (17):

$$\bar{u}_v^{n+1/2} = u_v^n + \frac{\Delta t}{2} (\Delta^v u_v^n + f_v^n),$$

or formula (18):

$$\bar{u}_v^{TT,n+1/2} = u_v^{TT,n} + \frac{\Delta t}{2} (\Delta^{v,TT} u_v^{TT,n} + f_v^{TT,n}),$$

with  $\Delta t/2$  instead of  $\Delta t$ ;

(2) *Implicit step*: use formula (20):

$$u_v^{n+1} - \frac{\Delta t}{2} (\Delta^v u_v^{n+1} + f_v^{n+1}) = \bar{u}_v^{n+1/2},$$

or formula (21):

$$u_v^{TT,n+1} - \frac{\Delta t}{2} (\Delta^{v,TT} u_v^{TT,n+1} + f_v^{TT,n+1}) = \bar{u}_v^{TT,n+1/2},$$

with  $\Delta t/2$  instead of  $\Delta t$ .

It is worth mentioning that the boundary conditions are set at the initial time  $t^n$  in the first explicit step and at time  $t^{n+1/2}$  in the second and last implicit step. Algorithm 4 in D provides implementation details on the update from  $u_v^{TT,n}$  to  $u_v^{TT,n+1}$ .

## 5.1 Matrix-free preconditioned conjugate gradient method

The PCG routine is detailed in Algorithm 1. This algorithm is an implementation of the Conjugate Gradient method, adapted to operate on vectors in the tensor-train format as described below and with the introduction of a rounding step for the rank growth control. We propose a possible preconditioning strategy for this algorithm, which applies independently to each TT core. Our thorough experimentation indicates that this approach performs effectively, and we present it as the practical method we employed for solving the linear systems arising from implicit and semi-implicit time-marching schemes. A theoretical investigation of this formulation within the framework of Krylov subspace methods is beyond the scope of this paper and will be addressed in future research.

We discuss here only the implicit/semi-implicit step for the tensor-train, as the full-grid case is similar. We initialize the algorithm with the field  $u_v^{TT,n+\tau}$ , where  $\tau = 1$  for the implicit Euler scheme, in which we use  $\Delta t$ , and  $\tau = 1/2$  for the semi-implicit Crank-Nicolson scheme, where we use  $\Delta t/2$  instead. The algorithm needs two external procedures, `Matrix_Vector_Product` and `Preconditioner`, and applies the rounding algorithm after every update of the solution  $u_v^{TT}$ , the auxiliary residual  $r_v^{TT}$ , and the conjugate direction  $p_v^{TT}$ . The procedure `Matrix_Vector_Product` applies the discrete heat operator to an input TT field  $p_v^{TT}$ , i.e.,  $p_v^{TT} \rightarrow (p_v^{TT} - \tau \Delta t \Delta^{v,TT} p_v^{TT})$ , where  $\Delta^{v,TT}$  is the discrete vertex Laplace operator defined in Section 3.

For this operator, we construct the preconditioner  $\mathbf{P}$  based on the following splitting of the Laplacian operator:

$$P = (\alpha I - \tau \Delta t P_x)(\alpha I - \tau \Delta t P_y)(\alpha I - \tau \Delta t P_z),$$

see [4, 28]. Here,  $P_\ell = \text{tridiag}(1, 2, 1)/h_\ell^2$  with  $\ell \in \{x, y, z\}$  represents the tridiagonal matrices corresponding to the standard 3-point stencil finite difference discretization of the univariate Laplacian operator. This construction effectively approximates the inverse of the heat operator by a product of one-dimensional operators. The procedure `Preconditioner` applies this preconditioner to the residual  $r_v^{TT}$ , returning the preconditioned vector field  $\zeta_v^{TT}$ . Applying the preconditioner  $P$  to  $r_v^{TT}$  involves solving the linear system:

$$\zeta_v^{TT} = P^{-1} r_v^{TT} = (I - \tau \Delta t P_z)^{-1} (I - \tau \Delta t P_y)^{-1} (I - \tau \Delta t P_x)^{-1} r_v^{TT}.$$

Consider the TT representations of  $\zeta_v^{TT}$  and  $r_v^{TT}$  (using the symbols  $\mathcal{Z}_\ell$  and  $\mathcal{R}_\ell$  to denote the respective cores):

$$\begin{aligned} \zeta_v^{TT}(i_v, j_v, k_v) &= \sum_{\alpha_1=1}^{r_1} \sum_{\alpha_2=1}^{r_2} \mathcal{Z}_1(i_v, \alpha_1) \mathcal{Z}_2(\alpha_1, j_v, \alpha_2) \mathcal{Z}_3(\alpha_2, k_v), \\ r_v^{TT}(i_v, j_v, k_v) &= \sum_{\alpha_1=1}^{r_1} \sum_{\alpha_2=1}^{r_2} \mathcal{R}_1(i_v, \alpha_1) \mathcal{R}_2(\alpha_1, j_v, \alpha_2) \mathcal{R}_3(\alpha_2, k_v), \end{aligned}$$

where  $\zeta_v^{TT}$  and  $r_v^{TT}$  have the same ranks  $r_1$  and  $r_2$ . The application of  $P$  reduces to solving a series of tridiagonal systems along each spatial dimension defined by the matrices  $P_x$ ,  $P_y$ , and  $P_z$  and the corresponding spatial fibers of  $r_v^{TT}$ . The

---

**Algorithm 1** Preconditioned Conjugate Gradient (PCG)

---

**Input:**

- $u_v^{TT, n+\tau}$ : vertex grid function at time  $t^{n+\tau}$ , with  $\tau \in \{1/2, 1\}$
- $b_v^{TT}$ : right-hand side function on  $\Omega$
- tol: tolerance
- maxiter: maximum number of iterations

**Output:**

- $u_v^{TT, n+1}$ : vertex grid function at time  $t^{n+1}$

```
1: procedure PCG( $u_v^{TT, n+\tau}, b_v^{TT}, \text{tol}, \text{maxiter}$ )  
2:    $u_v^{TT} \leftarrow u_v^{TT, n+\tau}$  ▷ Initial guess for the solution  
3:    $r_v^{TT} \leftarrow \text{rndg}(b_v^{TT} - \text{Matrix\_Vector\_Product}(u_v^{TT}))$  ▷ Initial residual  
4:    $\|r_v^{TT, 0}\| \leftarrow \|r_v^{TT}\|$  ▷ Compute & store the initial residual norm  
5:    $\zeta_v^{TT} \leftarrow \text{Preconditioner}(r_v^{TT})$  ▷ Apply preconditioner  
6:    $p_v^{TT} \leftarrow \zeta_v^{TT}$  ▷ Assign Initial search direction  
7:    $\rho \leftarrow r_v^{TT} \cdot \zeta_v^{TT}$   
8:   for  $\ell \leftarrow 1$  to maxiter do ▷ Krylov loop  
9:      $(Ap_v^{TT}) \leftarrow \text{Matrix\_Vector\_Product}(p_v^{TT})$  ▷ Matrix-vector product  
10:     $\alpha \leftarrow \rho / (p_v^{TT} \cdot (Ap_v^{TT}))$  ▷ Update  $\alpha$   
11:     $u_v^{TT} \leftarrow \text{rndg}(u_v^{TT} + \alpha p_v^{TT})$  ▷ Update solution  
12:     $r_v^{TT} \leftarrow \text{rndg}(r_v^{TT} - \alpha (Ap_v^{TT}))$  ▷ Update residual  
13:    if  $\|r_v^{TT}\| < \text{tol} \|r_v^{TT, 0}\|$  then ▷ Check convergence  
14:       $u_v^{TT, n+1} \leftarrow u_v^{TT}$   
15:      return  $u_v^{TT, n+1}$  ▷ Converged!  
16:    end if  
17:     $\zeta_v^{TT} \leftarrow \text{Preconditioner}(r_v^{TT})$  ▷ Apply preconditioner  
18:     $\rho_{\text{new}} \leftarrow r_v^{TT} \cdot \zeta_v^{TT}$  ▷ Update  $\rho$   
19:     $p_v^{TT} \leftarrow \text{rndg}(\zeta_v^{TT} + (\rho_{\text{new}}/\rho)p_v^{TT})$  ▷ Update conjugate direction  
20:     $\rho \leftarrow \rho_{\text{new}}$   
21:  end for  
22:   $u_v^{TT, n+1} \leftarrow u_v^{TT}$  ▷ Maximum iterations reached  
23: end procedure
```

---

cores of  $\zeta_v^{TT}$  are then given by:

$$\begin{aligned} \forall \alpha_1 = 1, 2, \dots, r_1, \quad \forall \alpha_2 = 1, 2, \dots, r_2 \\ \mathcal{Z}_1(:, \alpha_1) &= (I - \tau \Delta t P_x)^{-1} \mathcal{R}_1(:, \alpha_1), \\ \mathcal{Z}_2(\alpha_1, :, \alpha_2) &= (I - \tau \Delta t P_y)^{-1} \mathcal{R}_2(\alpha_1, :, \alpha_2), \\ \mathcal{Z}_3(\alpha_2, :) &= (I - \tau \Delta t P_z)^{-1} \mathcal{R}_3(\alpha_2, :). \end{aligned}$$

These tridiagonal systems can be efficiently solved using the Thomas algorithm [35].

## 6 Numerical Experiments

This section presents a numerical investigation of the tensor-train method developed in the previous sections applied to problem (1)-(2). To this end, we first verify the consistency of our Laplace operator approximation to confirm that the discretization error scales as  $\mathcal{O}(h^2)$  as expected when refining the mesh, where  $h_x = h_y = h_z := h$ . After this validation, we investigate the rank stability of the numerical approximate solution when problem (1)-(2) admits rank-1 solution. Finally, we evaluate the method's effectiveness using a manufactured solution, varying the initial approximation's rank to assess both the computational efficiency and accuracy of the proposed method.

To impose that  $h_x = h_y = h_z$ , we set  $N_c^x = N_c^y = N_c^z := N_c$  in all test cases. We consider a sequence of grid meshes defined on the unit cube  $\Omega = [0, 1]^3$ , starting from a  $20 \times 20 \times 20$  grid ( $N_c = 20$  and  $h = 1/N_c = 0.05$ ) with two additional boundary layers ( $N^{\text{bnd}} = 2$ ). We compare the FG and the TT implementations in three different scenarios:

- *regular grids*: tensor product grids with equispaced distributed vertices in each direction;
- *variable grids*: tensor product grids with variable mesh size in each direction, such as in Figure 4. In particular,  $h$  degrades by a factor of 1.125 in each direction, so that  $h_{x,0} = h$  and  $h_{x,i_c} = 1.125 h_{x,i_c-1}$  for each  $i_c$ , the same holding for  $h_{y,j_c}$  and  $h_{z,k_c}$ ;
- *remapped domains*: tensor product of equispaced distributed vertices on a remapped domain, as the one presented in Figure 5. The transformation gives the remapping:

$$(\tilde{x}, \tilde{y}, \tilde{z}) \rightarrow (-2e^{-2x}, -2e^{-2y}, -2e^{-2z}).$$

All errors are evaluated using the Frobenius norm suitably rescaled by  $h^{\frac{3}{2}}$ , to have a norm that is equivalent to a mesh-dependent  $L^2$ -like norm. In this section, we will label all the results from the full-grid implementations by “FG” and all the results from the tensor-train implementations by “TT”. Computations have been performed using a 3.60GHz Intel Core i7 processor with 16 cores and 32GB of RAM.

## 6.1 Consistency error evaluation

Let  $u(\mathbf{x})$  be a smooth enough function (at least  $C^2$ -regular),  $u_v$  the grid function that is obtained by sampling  $u$  at the grid nodes, and  $u_v^{TT}$  its tensor-train representation. We define the consistency error of the Laplace operator approximation at  $u$  as the residual norms

$$\mathcal{R}_v(u_v) = \|\Delta^v u_v - (\Delta u)|_v\| \quad \text{and} \quad \mathcal{R}_v(u_v^{TT}) = \|\Delta^{v,TT} u_v^{TT} - (\Delta u)|_v\|,$$

where  $(\Delta u)|_v = \{\Delta u(x_v, y_v, z_v)\}$ , the Laplacian of  $u$  evaluated at the grid nodes  $v$ . The consistency error is expected to scale as  $\mathcal{O}(h^2)$  when  $h$  is refined. We report the results for the approximation of the Laplacian of

$$u_1(x, y, z) = \sin(2\pi x) \sin(2\pi y) \sin(2\pi z), \quad x, y, z \in [0, 1], \quad (22)$$

in Table 1. We measure the residual norms  $\mathcal{R}_{v,FG}(u_v)$ ,  $\mathcal{R}_{v,TT}(u_v^{TT})$  relative to the full-grid and the tensor-train implementations, and their convergence rates, denoted as  $rate_{FG}$ ,  $rate_{TT}$ . We also report computational times ( $time_{FG}$ ,  $time_{TT}$ ) and storage ( $strg_{FG}$ ,  $strg_{TT}$ ), with ratios  $time_r = time_{FG}/time_{TT}$  and  $strg_r = strg_{FG}/strg_{TT}$ .

Both methods achieve almost the same consistency error levels and exhibit the expected second-order convergence rate in all the test cases, thus confirming the consistency of the TT Laplace operator. We also note that the TT solver outperforms the FG solver in storage requirements and computational time by multiple orders of magnitude, demonstrating the extraordinary efficiency of the TT approach.

## 6.2 Rank-1 solution approximations

As a second experiment, we consider the rank-1 and time-dependent solution

$$u_2(x, y, z, t) = \sin(2\pi x) \sin(2\pi y) \sin(2\pi z) \cos(2\pi t) \quad x, y, z, t \in [0, 1], \quad (23)$$

comparing the explicit Euler, implicit Euler, and Crank-Nicolson schemes with an initial time step equal to  $\Delta t = 10^{-4}$ . In this case, at each refinement level, in addition to halving the space size  $h$ , we divide  $\Delta t$  by a coefficient 4 in the explicit Euler method (for stability reasons) and by a coefficient 2 in the implicit Euler and semi-implicit Crank-Nicolson methods. The number of time steps  $N_{\Delta t}$  is set to  $1/\Delta t$ , ensuring that the simulation always reaches the final time  $T = 1$ . For computational reasons, in the last two time refinements of the FG implementation, we set  $N_{\Delta t} = 100$  and multiply the computational time by  $1/(\Delta t N_{\Delta t})$  to estimate the total computational time. We empirically observed that this approximation leads to an average 3% discrepancy compared with the actual computational time. The rounding threshold was set to  $\epsilon = 10^{-4}$ ; this constant affects the `rndg` procedure present in the setting of the boundary conditions, in PCG and in the update of the solution at each time step.

Table 1: Consistency error tests: residual  $\mathcal{R}_v$ , convergence rate  $rate$ , computational time  $time$ , and storage  $strg$  in FG and TT implementation, with ratios  $time_r = time_{FG}/time_{TT}$  and  $strg_r = strg_{FG}/strg_{TT}$ .

(a) Regular grids.

$h$	$\mathcal{R}_{v,FG}$	$\mathcal{R}_{v,TT}$	$rate_{FG}$	$rate_{TT}$	$time_{FG}$	$time_{TT}$	$time_r$	$strg_{FG}$	$strg_{TT}$	$strg_r$
$5.00 \cdot 10^{-2}$	$3.32 \cdot 10^0$	$3.32 \cdot 10^0$	—	—	$6.00 \cdot 10^0$	$0.00 \cdot 10^0$	$\infty$	$6.07 \cdot 10^4$	$2.75 \cdot 10^2$	$2.21 \cdot 10^2$
$2.50 \cdot 10^{-2}$	$8.53 \cdot 10^{-1}$	$8.53 \cdot 10^{-1}$	1.96	1.96	$4.60 \cdot 10^1$	$1.00 \cdot 10^0$	$4.60 \cdot 10^1$	$3.59 \cdot 10^5$	$4.95 \cdot 10^2$	$7.24 \cdot 10^2$
$1.25 \cdot 10^{-2}$	$2.15 \cdot 10^{-1}$	$2.15 \cdot 10^{-1}$	1.99	1.99	$1.79 \cdot 10^2$	$2.00 \cdot 10^0$	$8.95 \cdot 10^1$	$2.44 \cdot 10^6$	$9.35 \cdot 10^2$	$2.60 \cdot 10^3$
$6.25 \cdot 10^{-3}$	$5.38 \cdot 10^{-2}$	$5.38 \cdot 10^{-2}$	2.00	2.00	$1.58 \cdot 10^3$	$3.00 \cdot 10^0$	$5.26 \cdot 10^2$	$1.79 \cdot 10^7$	$1.82 \cdot 10^3$	$9.86 \cdot 10^3$
$3.13 \cdot 10^{-3}$	$1.35 \cdot 10^{-2}$	$1.35 \cdot 10^{-2}$	2.00	2.00	$1.88 \cdot 10^4$	$6.00 \cdot 10^0$	$3.13 \cdot 10^3$	$1.37 \cdot 10^8$	$3.58 \cdot 10^3$	$3.83 \cdot 10^4$

(b) Variable sized grids.

$h$	$\mathcal{R}_{v,FG}$	$\mathcal{R}_{v,TT}$	$rate_{FG}$	$rate_{TT}$	$time_{FG}$	$time_{TT}$	$time_r$	$strg_{FG}$	$strg_{TT}$	$strg_r$
$5.00 \cdot 10^{-2}$	$3.28 \cdot 10^0$	$3.31 \cdot 10^0$	—	—	$6.00 \cdot 10^0$	$1.00 \cdot 10^0$	$6.00 \cdot 10^0$	$6.07 \cdot 10^4$	$6.75 \cdot 10^2$	$8.99 \cdot 10^1$
$2.50 \cdot 10^{-2}$	$8.56 \cdot 10^{-1}$	$8.55 \cdot 10^{-1}$	1.94	1.95	$4.40 \cdot 10^1$	$1.00 \cdot 10^0$	$4.40 \cdot 10^1$	$3.59 \cdot 10^5$	$1.22 \cdot 10^3$	$2.95 \cdot 10^2$
$1.25 \cdot 10^{-2}$	$2.20 \cdot 10^{-1}$	$2.17 \cdot 10^{-1}$	1.96	1.98	$1.86 \cdot 10^2$	$3.00 \cdot 10^0$	$6.20 \cdot 10^1$	$2.44 \cdot 10^6$	$2.30 \cdot 10^3$	$1.06 \cdot 10^3$
$6.25 \cdot 10^{-3}$	$5.70 \cdot 10^{-2}$	$5.49 \cdot 10^{-2}$	1.95	1.98	$1.60 \cdot 10^3$	$4.00 \cdot 10^0$	$3.99 \cdot 10^2$	$1.79 \cdot 10^7$	$4.46 \cdot 10^3$	$4.02 \cdot 10^3$
$3.13 \cdot 10^{-3}$	$1.50 \cdot 10^{-2}$	$1.40 \cdot 10^{-2}$	1.93	1.97	$1.91 \cdot 10^4$	$1.50 \cdot 10^1$	$1.27 \cdot 10^3$	$1.37 \cdot 10^8$	$8.78 \cdot 10^3$	$1.56 \cdot 10^4$

(c) Remapped domains.

$h$	$\mathcal{R}_{v,FG}$	$\mathcal{R}_{v,TT}$	$rate_{FG}$	$rate_{TT}$	$time_{FG}$	$time_{TT}$	$time_r$	$strg_{FG}$	$strg_{TT}$	$strg_r$
$5.00 \cdot 10^{-2}$	$1.33 \cdot 10^1$	$1.33 \cdot 10^1$	—	—	$1.10 \cdot 10^1$	$1.00 \cdot 10^0$	$1.10 \cdot 10^1$	$6.07 \cdot 10^4$	$4.50 \cdot 10^2$	$1.35 \cdot 10^2$
$2.50 \cdot 10^{-2}$	$3.48 \cdot 10^0$	$3.48 \cdot 10^0$	1.93	1.93	$7.10 \cdot 10^1$	$1.00 \cdot 10^0$	$7.10 \cdot 10^1$	$3.59 \cdot 10^5$	$8.10 \cdot 10^2$	$4.43 \cdot 10^2$
$1.25 \cdot 10^{-2}$	$8.84 \cdot 10^{-1}$	$8.84 \cdot 10^{-1}$	1.98	1.98	$2.97 \cdot 10^2$	$2.00 \cdot 10^0$	$1.48 \cdot 10^2$	$2.44 \cdot 10^6$	$1.53 \cdot 10^3$	$1.59 \cdot 10^3$
$6.25 \cdot 10^{-3}$	$2.22 \cdot 10^{-1}$	$2.22 \cdot 10^{-1}$	1.99	1.99	$2.76 \cdot 10^3$	$4.00 \cdot 10^0$	$6.90 \cdot 10^2$	$1.79 \cdot 10^7$	$2.97 \cdot 10^3$	$6.02 \cdot 10^3$
$3.13 \cdot 10^{-3}$	$5.57 \cdot 10^{-2}$	$5.57 \cdot 10^{-2}$	2.00	2.00	$2.86 \cdot 10^4$	$1.50 \cdot 10^1$	$1.91 \cdot 10^3$	$1.37 \cdot 10^8$	$5.85 \cdot 10^3$	$2.34 \cdot 10^4$

The results for all tests are reported in Tables 2-3-4. In this case, and from now on, we measure the relative approximation errors  $\varepsilon_{FG} = \|u_v - u\|/\|u\|$  and  $\varepsilon_{TT} = \|u_v^{TT} - u\|/\|u\|$ . Since both the explicit and implicit Euler methods are only first-order in time, and the semi-implicit method is a second-order accurate method in time, we expect to see a convergence rate proportional to  $\mathcal{O}(h^2 + \Delta t)$  in the first case and an error scaling like  $\mathcal{O}(h^2 + \Delta t^2)$  in the second case. In the last two rows of each table, we report the estimated time values in italics, while all storage values are exact as they do not depend on the number of time steps.

The tensor-train reformulation demonstrates remarkable efficiency, while maintaining the same accuracy as the FG approach. Indeed, both methods exhibit optimal second-order convergence rates, as expected from the scheme construction, in all test cases, i.e., regular grids, variable-size grids along the Cartesian dimensions, and regular grids on remapped domains, and the three time-marching options of explicit, implicit, and semi-implicit schemes. However, the TT solver dramatically outperforms the FG solver in storage requirements and computational time by multiple orders of magnitude. In fact, we can see that:

- the computational time ratio (columns  $time_r = time_{FG}/time_{TT}$ ) increases from  $\mathcal{O}(10)$  to  $\mathcal{O}(10^3)$ , with greater benefits at finer resolutions.
- the storage ratio (columns  $strg_r = strg_{FG}/strg_{TT}$ ) increases consistently from  $\mathcal{O}(10)$  on the coarser grids to  $\mathcal{O}(10^4)$  on the finer grids;

Such efficiency gains are achieved without compromising accuracy, as shown by the error levels in the columns labeled by  $\varepsilon_{FG}$  and  $\varepsilon_{TT}$ , which are identical throughout all refined grid calculations.

As explained in Section 2, the maximum TT rank of  $u_v^{TT}$  plays a crucial role in the simulation, related to its accuracy and computational cost. Throughout Sections 3-4, we pointed out how some operations, e.g. the sums of derivative tensors, while not introducing additional errors in the TT representation of the finite difference approximation, may increase the rank thus requiring apposite rounding steps to keep our tensor-train representation “low-rank”. In Figure 5, we plot the maximum TT rank reached by  $u_v^{TT}$  throughout the whole simulation, relative to the regular grid scenario with the explicit and implicit Euler method (cf. Tables 2(a)-(b)). Each line corresponds to a different space refinement (the rows of Table 2), and the  $x$ -values indicate the advancement in time. Notably, the ranks do not increase in time, and finer grids lead to lower ranks; in fact, in the last two refinements, the rank is constantly equal to one. We refer to

Table 2: Rank-1 solution on regular grids: relative error  $\varepsilon$ , convergence rate  $rate$ , computational time  $time$ , and storage  $strg$  in FG and TT implementation, with ratios  $time_r = time_{FG}/time_{TT}$  and  $strg_r = strg_{FG}/strg_{TT}$ .

(a) Explicit Euler method.

$h$	$\Delta t$	$\varepsilon_{FG}$	$\varepsilon_{TT}$	$rate_{FG}$	$rate_{TT}$	$time_{FG}$	$time_{TT}$	$time_r$	$strg_{FG}$	$strg_{TT}$	$strg_r$
$5.00 \cdot 10^{-2}$	$1.00 \cdot 10^{-4}$	$9.43 \cdot 10^{-2}$	$9.43 \cdot 10^{-2}$	—	—	$2.76 \cdot 10^4$	$1.89 \cdot 10^4$	$1.46 \cdot 10^0$	$6.07 \cdot 10^4$	$8.00 \cdot 10^2$	$7.59 \cdot 10^1$
$2.50 \cdot 10^{-2}$	$2.50 \cdot 10^{-5}$	$2.18 \cdot 10^{-2}$	$2.18 \cdot 10^{-2}$	2.11	2.12	$8.02 \cdot 10^5$	$1.09 \cdot 10^5$	$7.34 \cdot 10^0$	$3.59 \cdot 10^5$	$1.35 \cdot 10^3$	$2.66 \cdot 10^2$
$1.25 \cdot 10^{-2}$	$6.25 \cdot 10^{-6}$	$5.27 \cdot 10^{-3}$	$5.26 \cdot 10^{-3}$	2.05	2.05	$2.59 \cdot 10^7$	$5.33 \cdot 10^5$	$4.86 \cdot 10^1$	$2.44 \cdot 10^6$	$1.53 \cdot 10^3$	$1.59 \cdot 10^3$
$6.25 \cdot 10^{-3}$	$1.56 \cdot 10^{-6}$	—	$1.30 \cdot 10^{-3}$	—	2.02	$9.53 \cdot 10^8$	$2.37 \cdot 10^6$	$4.02 \cdot 10^2$	$1.79 \cdot 10^7$	$2.64 \cdot 10^3$	$6.78 \cdot 10^3$
$3.13 \cdot 10^{-3}$	$3.91 \cdot 10^{-7}$	—	$3.22 \cdot 10^{-4}$	—	2.01	$4.66 \cdot 10^{10}$	$2.04 \cdot 10^7$	$2.28 \cdot 10^3$	$1.37 \cdot 10^8$	$5.20 \cdot 10^3$	$2.63 \cdot 10^4$

(b) Implicit Euler method.

$h$	$\Delta t$	$\varepsilon_{FG}$	$\varepsilon_{TT}$	$rate_{FG}$	$rate_{TT}$	$time_{FG}$	$time_{TT}$	$time_r$	$strg_{FG}$	$strg_{TT}$	$strg_r$
$5.00 \cdot 10^{-2}$	$1.00 \cdot 10^{-4}$	$9.43 \cdot 10^{-2}$	$9.43 \cdot 10^{-2}$	—	—	$4.50 \cdot 10^4$	$3.36 \cdot 10^4$	$1.34 \cdot 10^0$	$6.07 \cdot 10^4$	$9.75 \cdot 10^2$	$6.23 \cdot 10^1$
$2.50 \cdot 10^{-2}$	$5.00 \cdot 10^{-5}$	$2.18 \cdot 10^{-2}$	$2.18 \cdot 10^{-2}$	2.11	2.12	$6.09 \cdot 10^5$	$8.48 \cdot 10^4$	$7.18 \cdot 10^0$	$3.59 \cdot 10^5$	$8.10 \cdot 10^2$	$4.43 \cdot 10^2$
$1.25 \cdot 10^{-2}$	$2.50 \cdot 10^{-5}$	$5.27 \cdot 10^{-3}$	$5.25 \cdot 10^{-3}$	2.05	2.05	$9.65 \cdot 10^6$	$2.96 \cdot 10^5$	$3.26 \cdot 10^1$	$2.44 \cdot 10^6$	$1.36 \cdot 10^3$	$1.79 \cdot 10^3$
$6.25 \cdot 10^{-3}$	$1.25 \cdot 10^{-5}$	—	$1.30 \cdot 10^{-3}$	—	2.02	$1.83 \cdot 10^8$	$6.02 \cdot 10^5$	$3.04 \cdot 10^2$	$1.79 \cdot 10^7$	$1.82 \cdot 10^3$	$9.86 \cdot 10^3$
$3.13 \cdot 10^{-3}$	$6.25 \cdot 10^{-6}$	—	$3.21 \cdot 10^{-4}$	—	2.01	$4.52 \cdot 10^9$	$2.25 \cdot 10^6$	$2.01 \cdot 10^3$	$1.37 \cdot 10^8$	$1.95 \cdot 10^3$	$7.03 \cdot 10^4$

(c) Crank-Nicolson method.

$h$	$\Delta t$	$\varepsilon_{FG}$	$\varepsilon_{TT}$	$rate_{FG}$	$rate_{TT}$	$time_{FG}$	$time_{TT}$	$time_r$	$strg_{FG}$	$strg_{TT}$	$strg_r$
$5.00 \cdot 10^{-2}$	$1.00 \cdot 10^{-4}$	$6.81 \cdot 10^{-2}$	$9.43 \cdot 10^{-2}$	—	—	$9.33 \cdot 10^4$	$5.49 \cdot 10^4$	$1.70 \cdot 10^0$	$6.07 \cdot 10^4$	$9.75 \cdot 10^2$	$6.23 \cdot 10^1$
$2.50 \cdot 10^{-2}$	$5.00 \cdot 10^{-5}$	$1.30 \cdot 10^{-2}$	$2.18 \cdot 10^{-2}$	2.39	2.11	$1.30 \cdot 10^6$	$1.40 \cdot 10^5$	$9.30 \cdot 10^0$	$3.59 \cdot 10^5$	$8.10 \cdot 10^2$	$4.43 \cdot 10^2$
$1.25 \cdot 10^{-2}$	$2.50 \cdot 10^{-5}$	$2.94 \cdot 10^{-3}$	$5.26 \cdot 10^{-3}$	2.14	2.05	$2.11 \cdot 10^7$	$4.41 \cdot 10^5$	$4.78 \cdot 10^1$	$2.44 \cdot 10^6$	$1.36 \cdot 10^3$	$1.79 \cdot 10^3$
$6.25 \cdot 10^{-3}$	$1.25 \cdot 10^{-5}$	—	$1.30 \cdot 10^{-3}$	—	2.02	$4.13 \cdot 10^8$	$8.99 \cdot 10^5$	$4.60 \cdot 10^2$	$1.79 \cdot 10^7$	$9.90 \cdot 10^2$	$1.81 \cdot 10^4$
$3.13 \cdot 10^{-3}$	$6.25 \cdot 10^{-6}$	—	$3.22 \cdot 10^{-4}$	—	2.01	$1.07 \cdot 10^{10}$	$3.77 \cdot 10^6$	$2.84 \cdot 10^3$	$1.37 \cdot 10^8$	$3.58 \cdot 10^3$	$3.83 \cdot 10^4$

Table 3: Rank-1 solution on variable sized grids: relative error  $\varepsilon$ , convergence rate  $rate$ , computational time  $time$ , and storage  $strg$  in FG and TT implementation, with ratios  $time_r = time_{FG}/time_{TT}$  and  $strg_r = strg_{FG}/strg_{TT}$ .

(a) Explicit Euler method.

$h$	$\Delta t$	$\varepsilon_{FG}$	$\varepsilon_{TT}$	$rate_{FG}$	$rate_{TT}$	$time_{FG}$	$time_{TT}$	$time_r$	$strg_{FG}$	$strg_{TT}$	$strg_r$
$5.00 \cdot 10^{-2}$	$1.00 \cdot 10^{-4}$	$9.34 \cdot 10^{-2}$	$9.51 \cdot 10^{-2}$	—	—	$2.76 \cdot 10^4$	$2.13 \cdot 10^4$	$1.30 \cdot 10^0$	$6.07 \cdot 10^4$	$1.25 \cdot 10^3$	$4.86 \cdot 10^1$
$2.50 \cdot 10^{-2}$	$2.50 \cdot 10^{-5}$	$2.17 \cdot 10^{-2}$	$2.21 \cdot 10^{-2}$	2.10	2.11	$8.01 \cdot 10^5$	$1.34 \cdot 10^5$	$5.96 \cdot 10^0$	$3.59 \cdot 10^5$	$1.44 \cdot 10^3$	$2.49 \cdot 10^2$
$1.25 \cdot 10^{-2}$	$6.25 \cdot 10^{-6}$	$5.28 \cdot 10^{-3}$	$5.34 \cdot 10^{-3}$	2.04	2.05	$2.61 \cdot 10^7$	$5.40 \cdot 10^5$	$4.84 \cdot 10^1$	$2.44 \cdot 10^6$	$1.96 \cdot 10^3$	$1.25 \cdot 10^3$
$6.25 \cdot 10^{-3}$	$1.56 \cdot 10^{-6}$	—	$1.31 \cdot 10^{-3}$	—	2.02	$9.40 \cdot 10^8$	$2.40 \cdot 10^6$	$3.92 \cdot 10^2$	$1.79 \cdot 10^7$	$2.64 \cdot 10^3$	$6.78 \cdot 10^3$
$3.13 \cdot 10^{-3}$	$3.91 \cdot 10^{-7}$	—	$3.28 \cdot 10^{-4}$	—	2.00	$4.56 \cdot 10^{10}$	$2.11 \cdot 10^7$	$2.16 \cdot 10^3$	$1.37 \cdot 10^8$	$5.20 \cdot 10^3$	$2.63 \cdot 10^4$

(b) Implicit Euler method.

$h$	$\Delta t$	$\varepsilon_{FG}$	$\varepsilon_{TT}$	$rate_{FG}$	$rate_{TT}$	$time_{FG}$	$time_{TT}$	$time_r$	$strg_{FG}$	$strg_{TT}$	$strg_r$
$5.00 \cdot 10^{-2}$	$1.00 \cdot 10^{-4}$	$9.33 \cdot 10^{-2}$	$9.50 \cdot 10^{-2}$	—	—	$4.46 \cdot 10^4$	$5.30 \cdot 10^4$	$8.43 \cdot 10^{-1}$	$6.07 \cdot 10^4$	$9.75 \cdot 10^2$	$6.23 \cdot 10^1$
$2.50 \cdot 10^{-2}$	$5.00 \cdot 10^{-5}$	$2.17 \cdot 10^{-2}$	$2.20 \cdot 10^{-2}$	2.10	2.11	$6.03 \cdot 10^5$	$1.12 \cdot 10^5$	$5.40 \cdot 10^0$	$3.59 \cdot 10^5$	$8.10 \cdot 10^2$	$4.43 \cdot 10^2$
$1.25 \cdot 10^{-2}$	$2.50 \cdot 10^{-5}$	$5.27 \cdot 10^{-3}$	$5.33 \cdot 10^{-3}$	2.04	2.05	$9.50 \cdot 10^6$	$3.10 \cdot 10^5$	$3.06 \cdot 10^1$	$2.44 \cdot 10^6$	$1.53 \cdot 10^3$	$1.59 \cdot 10^3$
$6.25 \cdot 10^{-3}$	$1.25 \cdot 10^{-5}$	—	$1.32 \cdot 10^{-3}$	—	2.02	$1.78 \cdot 10^8$	$5.34 \cdot 10^5$	$3.33 \cdot 10^2$	$1.79 \cdot 10^7$	$2.97 \cdot 10^3$	$6.03 \cdot 10^3$
$3.13 \cdot 10^{-3}$	$6.25 \cdot 10^{-6}$	—	$3.28 \cdot 10^{-4}$	—	2.01	$4.46 \cdot 10^9$	$2.17 \cdot 10^6$	$2.06 \cdot 10^3$	$1.37 \cdot 10^8$	$5.85 \cdot 10^3$	$2.34 \cdot 10^4$

(c) Crank-Nicolson method.

$h$	$\Delta t$	$\varepsilon_{FG}$	$\varepsilon_{TT}$	$rate_{FG}$	$rate_{TT}$	$time_{FG}$	$time_{TT}$	$time_r$	$strg_{FG}$	$strg_{TT}$	$strg_r$
$5.00 \cdot 10^{-2}$	$1.00 \cdot 10^{-4}$	$9.33 \cdot 10^{-2}$	$9.50 \cdot 10^{-2}$	—	—	$7.41 \cdot 10^4$	$7.84 \cdot 10^4$	$9.45 \cdot 10^{-1}$	$6.07 \cdot 10^4$	$9.75 \cdot 10^2$	$6.23 \cdot 10^1$
$2.50 \cdot 10^{-2}$	$5.00 \cdot 10^{-5}$	$2.17 \cdot 10^{-2}$	$2.21 \cdot 10^{-2}$	2.10	2.11	$1.02 \cdot 10^6$	$1.22 \cdot 10^5$	$8.34 \cdot 10^0$	$3.59 \cdot 10^5$	$1.04 \cdot 10^3$	$3.46 \cdot 10^2$
$1.25 \cdot 10^{-2}$	$2.50 \cdot 10^{-5}$	$5.28 \cdot 10^{-3}$	$5.34 \cdot 10^{-3}$	2.04	2.05	$1.61 \cdot 10^7$	$4.46 \cdot 10^5$	$3.61 \cdot 10^1$	$2.44 \cdot 10^6$	$1.53 \cdot 10^3$	$1.59 \cdot 10^3$
$6.25 \cdot 10^{-3}$	$1.25 \cdot 10^{-5}$	—	$1.32 \cdot 10^{-3}$	—	2.02	$2.96 \cdot 10^8$	$8.56 \cdot 10^5$	$3.46 \cdot 10^2$	$1.79 \cdot 10^7$	$2.97 \cdot 10^3$	$6.03 \cdot 10^3$
$3.13 \cdot 10^{-3}$	$6.25 \cdot 10^{-6}$	—	$3.29 \cdot 10^{-4}$	—	2.00	$7.27 \cdot 10^9$	$3.64 \cdot 10^6$	$2.00 \cdot 10^3$	$1.37 \cdot 10^8$	$5.85 \cdot 10^3$	$2.34 \cdot 10^4$

Table 4: Rank-1 solution on remapped domains: relative error  $\varepsilon$ , convergence rate  $rate$ , computational time  $time$ , and storage  $strg$  in FG and TT implementation, with ratios  $time_r = time_{FG}/time_{TT}$  and  $strg_r = strg_{FG}/strg_{TT}$ .

(a) Explicit Euler method.

$h$	$\Delta t$	$\varepsilon_{FG}$	$\varepsilon_{TT}$	$rate_{FG}$	$rate_{TT}$	$time_{FG}$	$time_{TT}$	$time_r$	$strg_{FG}$	$strg_{TT}$	$strg_r$
$5.00 \cdot 10^{-2}$	$1.00 \cdot 10^{-4}$	$9.40 \cdot 10^{-2}$	$9.30 \cdot 10^{-2}$	—	—	$4.80 \cdot 10^4$	$3.60 \cdot 10^4$	$1.33 \cdot 10^0$	$6.07 \cdot 10^4$	$1.50 \cdot 10^3$	$4.05 \cdot 10^1$
$2.50 \cdot 10^{-2}$	$2.50 \cdot 10^{-5}$	$1.99 \cdot 10^{-2}$	$1.96 \cdot 10^{-2}$	2.24	2.24	$1.47 \cdot 10^6$	$2.89 \cdot 10^5$	$5.08 \cdot 10^0$	$3.59 \cdot 10^5$	$2.16 \cdot 10^3$	$1.66 \cdot 10^2$
$1.25 \cdot 10^{-2}$	$6.25 \cdot 10^{-6}$	$4.66 \cdot 10^{-3}$	$4.64 \cdot 10^{-3}$	2.09	2.08	$4.80 \cdot 10^7$	$1.15 \cdot 10^6$	$4.17 \cdot 10^1$	$2.44 \cdot 10^6$	$2.55 \cdot 10^3$	$9.55 \cdot 10^2$
$6.25 \cdot 10^{-3}$	$1.56 \cdot 10^{-6}$	—	$1.12 \cdot 10^{-3}$	—	2.06	$1.66 \cdot 10^9$	$6.45 \cdot 10^6$	$2.57 \cdot 10^2$	$1.79 \cdot 10^7$	$8.25 \cdot 10^3$	$2.17 \cdot 10^3$
$3.13 \cdot 10^{-3}$	$3.91 \cdot 10^{-7}$	—	$2.76 \cdot 10^{-4}$	—	2.01	$7.33 \cdot 10^{10}$	$8.04 \cdot 10^7$	$9.11 \cdot 10^2$	$1.37 \cdot 10^8$	$1.04 \cdot 10^4$	$1.32 \cdot 10^4$

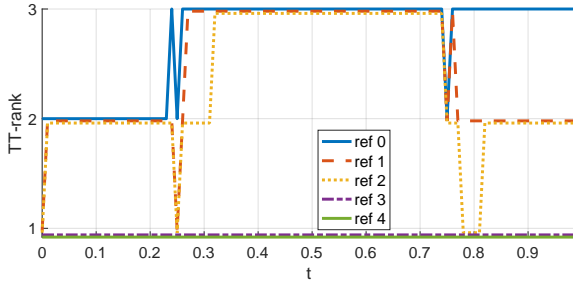
(b) Implicit Euler method.

$h$	$\Delta t$	$\varepsilon_{FG}$	$\varepsilon_{TT}$	$rate_{FG}$	$rate_{TT}$	$time_{FG}$	$time_{TT}$	$time_r$	$strg_{FG}$	$strg_{TT}$	$strg_r$
$5.00 \cdot 10^{-2}$	$1.00 \cdot 10^{-4}$	$9.39 \cdot 10^{-2}$	$9.24 \cdot 10^{-2}$	—	—	$6.83 \cdot 10^4$	$1.96 \cdot 10^5$	$3.48 \cdot 10^{-1}$	$6.07 \cdot 10^4$	$9.75 \cdot 10^2$	$6.23 \cdot 10^1$
$2.50 \cdot 10^{-2}$	$5.00 \cdot 10^{-5}$	$1.99 \cdot 10^{-2}$	$1.93 \cdot 10^{-2}$	2.24	2.26	$9.83 \cdot 10^5$	$5.95 \cdot 10^5$	$1.65 \cdot 10^0$	$3.59 \cdot 10^5$	$1.44 \cdot 10^3$	$2.49 \cdot 10^2$
$1.25 \cdot 10^{-2}$	$2.50 \cdot 10^{-5}$	$4.64 \cdot 10^{-3}$	$4.61 \cdot 10^{-3}$	2.10	2.06	$1.59 \cdot 10^7$	$7.27 \cdot 10^5$	$2.19 \cdot 10^1$	$2.44 \cdot 10^6$	$1.96 \cdot 10^3$	$1.25 \cdot 10^3$
$6.25 \cdot 10^{-3}$	$1.25 \cdot 10^{-5}$	—	$1.13 \cdot 10^{-3}$	—	2.03	$3.14 \cdot 10^8$	$2.83 \cdot 10^6$	$1.11 \cdot 10^2$	$1.79 \cdot 10^7$	$2.97 \cdot 10^3$	$6.03 \cdot 10^3$
$3.13 \cdot 10^{-3}$	$6.25 \cdot 10^{-6}$	—	$2.78 \cdot 10^{-4}$	—	2.02	$8.74 \cdot 10^9$	$3.34 \cdot 10^7$	$2.62 \cdot 10^2$	$1.37 \cdot 10^8$	$5.85 \cdot 10^3$	$2.34 \cdot 10^4$

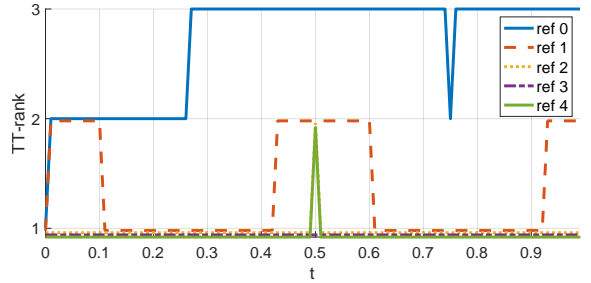
(c) Crank-Nicolson method.

$h$	$\Delta t$	$\varepsilon_{FG}$	$\varepsilon_{TT}$	$rate_{FG}$	$rate_{TT}$	$time_{FG}$	$time_{TT}$	$time_r$	$strg_{FG}$	$strg_{TT}$	$strg_r$
$5.00 \cdot 10^{-2}$	$1.00 \cdot 10^{-4}$	$9.40 \cdot 10^{-2}$	$9.22 \cdot 10^{-2}$	—	—	$1.16 \cdot 10^5$	$1.92 \cdot 10^5$	$6.04 \cdot 10^{-1}$	$6.07 \cdot 10^4$	$7.50 \cdot 10^2$	$8.09 \cdot 10^1$
$2.50 \cdot 10^{-2}$	$5.00 \cdot 10^{-5}$	$1.99 \cdot 10^{-2}$	$1.95 \cdot 10^{-2}$	2.24	2.24	$1.71 \cdot 10^6$	$4.47 \cdot 10^5$	$3.84 \cdot 10^0$	$3.59 \cdot 10^5$	$1.76 \cdot 10^3$	$2.04 \cdot 10^2$
$1.25 \cdot 10^{-2}$	$2.50 \cdot 10^{-5}$	$4.66 \cdot 10^{-3}$	$4.62 \cdot 10^{-3}$	2.09	2.07	$2.76 \cdot 10^7$	$8.57 \cdot 10^5$	$3.22 \cdot 10^1$	$2.44 \cdot 10^6$	$2.55 \cdot 10^3$	$9.55 \cdot 10^2$
$6.25 \cdot 10^{-3}$	$1.25 \cdot 10^{-5}$	—	$1.13 \cdot 10^{-3}$	—	2.03	$5.09 \cdot 10^8$	$1.90 \cdot 10^6$	$2.67 \cdot 10^2$	$1.79 \cdot 10^7$	$3.80 \cdot 10^3$	$4.72 \cdot 10^3$
$3.13 \cdot 10^{-3}$	$6.25 \cdot 10^{-6}$	—	$2.83 \cdot 10^{-4}$	—	2.00	$1.31 \cdot 10^{10}$	$4.34 \cdot 10^7$	$3.02 \cdot 10^2$	$1.37 \cdot 10^8$	$1.40 \cdot 10^4$	$9.80 \cdot 10^3$

this phenomenon as the “rank stability” of the algorithm, and it indicates that our implementation can keep a low-rank representation of a low-rank solution during the whole time integration.



(a) explicit Euler method



(b) implicit Euler method

Table 5: Maximum rank of  $u_v^{TT}$  in each refinement step of the Euler method for rank-1 solution on regular grids. Plot values have been slightly shifted vertically to improve readability.

Last, we investigate the impact of the preconditioner on the condition number  $\kappa(A) = \lambda_{\max}(A)/\lambda_{\min}(A)$  of the global stiffness “matrix”  $A = I - \Delta t \Delta^{v,TT}$  that we use in the tensor-train implementation of the Euler implicit method (the same argument holds for the Crank-Nicolson semi-implicit method). Being  $A$  a perturbation of the identity “matrix”  $I$  for small  $\Delta t$ , we find that the minimum eigenvalue of  $A$  is  $\lambda_{\min}(A) \simeq 1$ , so that we can (roughly) estimate the condition numbers  $\kappa(A)$  and  $\kappa(P^{-1}AP)$  by computing only  $\lambda_{\max}(A)$  and  $\lambda_{\max}(P^{-1}AP)$  through the power method, see [14, Chapter 7.3]. Note that the power method only requires the matrix-vector product operation that we can perform by applying the routine `Matrix_Vector_Product`, cf. Section 5.1. In Table 6, we consider the results obtained for a sequence of refined regular grids for different values of  $\Delta t$ , e.g.,  $\Delta t \in \{1, 0.1, 0.01\}$ . We compare the maximum eigenvalue of the “plain matrix”  $A$  and the “preconditioned matrix”  $P^{-1}AP$  for decreasing  $h$  values. If  $\Delta t$  is sufficiently small, the stiffness “matrix” almost reduces to the identity “matrix” and both  $\lambda_{\max}(A)$  and  $\lambda_{\max}(P^{-1}AP)$  remain small, while bigger time steps lead to a significant growth of the maximum eigenvalue in the non-preconditioned case. The PCG effectively addresses this undesirable effect, maintaining  $\lambda_{\max}(P^{-1}AP) \simeq 1$ . Importantly, the use of the preconditioner



strongly mitigates the correlation between  $\lambda_{\max}(P^{-1}AP)$  and  $h$ , thus allowing the solver to work easily with much smaller mesh sizes.

Table 6: Maximum eigenvalue  $\lambda_{\max}$  of the stiffness matrix  $A$ , with and without preconditioner  $P$ , using different time steps  $\Delta t$ .

	$\Delta t = 1$		$\Delta t = 0.1$		$\Delta t = 0.01$	
$h$	$\lambda_{\max}(A)$	$\lambda_{\max}(P^{-1}AP)$	$\lambda_{\max}(A)$	$\lambda_{\max}(P^{-1}AP)$	$\lambda_{\max}(A)$	$\lambda_{\max}(P^{-1}AP)$
$2.00 \cdot 10^{-1}$	24.89	3.59	3.36	1.21	1.02	1.01
$1.00 \cdot 10^{-1}$	54.91	5.40	6.17	1.43	1.46	1.04
$5.00 \cdot 10^{-2}$	101.95	5.09	11.51	1.41	1.96	1.04
$2.50 \cdot 10^{-2}$	223.72	3.78	23.17	1.28	3.05	1.04
$1.25 \cdot 10^{-2}$	450.02	2.63	45.26	1.16	5.29	1.03
$6.30 \cdot 10^{-3}$	898.99	1.89	91.11	1.09	9.77	1.03

### 6.3 Rank-stable approximations of a general solution

As a further experiment, on a sequence of regular grids we consider the more general solution

$$u_3(x, y, z, t) = e^{-(x+y+z-\frac{3}{2})^2} t, \quad x, y, z, t \in [0, 1]. \quad (24)$$

In the case of high-rank solutions, a bad choice of the ranks for the initial approximations may compromise the accuracy of the entire simulation. From an initial calculation, we found that the grid function obtained by sampling only the space-dependent part of  $u_3(x, y, z, t)$  can be represented in tensor-train format with TT ranks equal to 11 and with an approximation error of the order of the machine precision. Then, in a set of preliminary tests (the results of which are not reported) we discovered that an initial solution approximated with ranks strictly less than 5 leads to bad approximations. We also noticed that having to deal with higher function ranks, the rounding threshold used in the tests of Section 6.2 was not small enough to provide accurate results. Therefore, we consider the three different initial ranks 5, 11, and 15, with  $\epsilon = 10^{-7}$ . In Table 7, we report the results for the explicit Euler method. As in Section 6.2, we start with  $h = 0.05$  and  $\Delta t = 10^{-4}$ , halving both of them at each refinement level, with  $N_{\Delta t} = 1000$  time steps.

Table 7: General solution on regular grids, explicit Euler method: relative error  $\varepsilon$ , convergence rate  $rate$ , computational time  $time$ , and storage  $strg$  in FG and TT implementation, with ratios  $time_r = time_{FG}/time_{TT}$  and  $strg_r = strg_{FG}/strg_{TT}$ .

(a) Initial rank = 5.

$h$	$\Delta t$	$\varepsilon_{FG}$	$\varepsilon_{TT}$	$rate_{FG}$	$rate_{TT}$	$time_{FG}$	$time_{TT}$	$time_r$	$strg_{FG}$	$strg_{TT}$	$strg_r$
$5.00 \cdot 10^{-2}$	$1.00 \cdot 10^{-4}$	$1.02 \cdot 10^{-3}$	$9.46 \cdot 10^{-4}$	—	—	$2.09 \cdot 10^3$	$1.35 \cdot 10^4$	$1.55 \cdot 10^{-1}$	$6.07 \cdot 10^4$	$4.05 \cdot 10^3$	$1.50 \cdot 10^1$
$2.50 \cdot 10^{-2}$	$2.50 \cdot 10^{-5}$	$2.34 \cdot 10^{-4}$	$2.08 \cdot 10^{-4}$	2.12	2.18	$6.16 \cdot 10^4$	$8.45 \cdot 10^4$	$7.29 \cdot 10^{-1}$	$3.59 \cdot 10^5$	$5.76 \cdot 10^3$	$6.23 \cdot 10^1$
$1.25 \cdot 10^{-2}$	$6.25 \cdot 10^{-6}$	$5.62 \cdot 10^{-5}$	$6.34 \cdot 10^{-5}$	2.06	1.72	$1.98 \cdot 10^6$	$6.70 \cdot 10^5$	$2.95 \cdot 10^0$	$2.44 \cdot 10^6$	$8.33 \cdot 10^3$	$2.92 \cdot 10^2$
$6.25 \cdot 10^{-3}$	$1.56 \cdot 10^{-6}$	$1.38 \cdot 10^{-5}$	$4.17 \cdot 10^{-3}$	2.03	-6.04	$7.77 \cdot 10^7$	$2.34 \cdot 10^7$	$3.32 \cdot 10^0$	$1.79 \cdot 10^7$	$2.49 \cdot 10^4$	$7.18 \cdot 10^2$

(b) Initial rank = 11.

$h$	$\Delta t$	$\varepsilon_{FG}$	$\varepsilon_{TT}$	$rate_{FG}$	$rate_{TT}$	$time_{FG}$	$time_{TT}$	$time_r$	$strg_{FG}$	$strg_{TT}$	$strg_r$
$5.00 \cdot 10^{-2}$	$1.00 \cdot 10^{-4}$	$1.02 \cdot 10^{-3}$	$9.49 \cdot 10^{-4}$	—	—	$2.09 \cdot 10^3$	$3.60 \cdot 10^4$	$5.81 \cdot 10^{-2}$	$6.07 \cdot 10^4$	$4.73 \cdot 10^3$	$1.28 \cdot 10^1$
$2.50 \cdot 10^{-2}$	$2.50 \cdot 10^{-5}$	$2.34 \cdot 10^{-4}$	$2.10 \cdot 10^{-4}$	2.12	2.17	$6.16 \cdot 10^4$	$2.39 \cdot 10^5$	$2.58 \cdot 10^{-1}$	$3.59 \cdot 10^5$	$5.76 \cdot 10^3$	$6.23 \cdot 10^1$
$1.25 \cdot 10^{-2}$	$6.25 \cdot 10^{-6}$	$5.62 \cdot 10^{-5}$	$5.11 \cdot 10^{-5}$	2.06	2.04	$1.98 \cdot 10^6$	$1.94 \cdot 10^6$	$1.02 \cdot 10^0$	$2.44 \cdot 10^6$	$1.09 \cdot 10^4$	$2.24 \cdot 10^2$
$6.25 \cdot 10^{-3}$	$1.56 \cdot 10^{-6}$	$1.38 \cdot 10^{-5}$	$1.29 \cdot 10^{-5}$	2.03	1.98	$7.77 \cdot 10^7$	$2.44 \cdot 10^7$	$3.19 \cdot 10^0$	$1.79 \cdot 10^7$	$2.11 \cdot 10^4$	$8.47 \cdot 10^2$

(c) Initial rank = 15.

$h$	$\Delta t$	$\varepsilon_{FG}$	$\varepsilon_{TT}$	$rate_{FG}$	$rate_{TT}$	$time_{FG}$	$time_{TT}$	$time_r$	$strg_{FG}$	$strg_{TT}$	$strg_r$
$5.00 \cdot 10^{-2}$	$1.00 \cdot 10^{-4}$	$1.02 \cdot 10^{-3}$	NaN	—	—	$2.09 \cdot 10^3$	$2.30 \cdot 10^6$	$9.07 \cdot 10^{-4}$	$6.07 \cdot 10^4$	$5.41 \cdot 10^5$	$1.12 \cdot 10^{-1}$
$2.50 \cdot 10^{-2}$	$2.50 \cdot 10^{-5}$	$2.34 \cdot 10^{-4}$	$2.10 \cdot 10^{-4}$	2.12	NaN	$6.16 \cdot 10^4$	$4.59 \cdot 10^5$	$1.34 \cdot 10^{-1}$	$3.59 \cdot 10^5$	$5.76 \cdot 10^3$	$6.23 \cdot 10^1$
$1.25 \cdot 10^{-2}$	$6.25 \cdot 10^{-6}$	$5.62 \cdot 10^{-5}$	$5.11 \cdot 10^{-5}$	2.06	2.04	$1.98 \cdot 10^6$	$3.56 \cdot 10^6$	$5.56 \cdot 10^{-1}$	$2.44 \cdot 10^6$	$1.09 \cdot 10^4$	$2.24 \cdot 10^2$
$6.25 \cdot 10^{-3}$	$1.56 \cdot 10^{-6}$	$1.38 \cdot 10^{-5}$	$1.29 \cdot 10^{-5}$	2.03	1.98	$7.77 \cdot 10^7$	$3.47 \cdot 10^7$	$2.24 \cdot 10^0$	$1.79 \cdot 10^7$	$2.11 \cdot 10^4$	$8.47 \cdot 10^2$

Using an initial rank of 5 leads to smaller tensors and, therefore, faster performance. However, after some refinements, such a small rank is not enough to preserve the accuracy required by the scheme, and the convergence deteriorates. With an initial rank of 11 instead, the error decreases as expected, and the method converges with the correct rate. After a few space refinements, the computational time ratio becomes favorable to the TT solver, while the storage required by the TT implementation is always much smaller compared to the FG. Last, using a higher initial rank implies more expensive computations and does not improve the solution accuracy. In the first line of Table 7(c) we see how the TT implementation failed to compute an approximation of  $u$  because the cross-interpolation was unable to approximate  $u$  on a coarse grid with a high rank. The smaller speed-up observed with higher ranks compared to the lower rank case can be explained by the fact that operations with higher rank tensors require more floating point operations, partially offsetting the advantage of using the tensor-train format.

## 6.4 Discussion

The performance of the previous sections demonstrates that the TT approach offers a robust and highly efficient alternative to traditional full-grid solvers while preserving the desired numerical properties. The usage of this type of representation leads to massive time and memory savings while guaranteeing almost identical accuracy with respect to the full-grid approach. However, the implementation based on the tensor-train format implies additional costs since it requires more sophisticated data structures and a redesign of the numerical algorithms for handling operations in the tensor format. While this additional complexity of the PDE solvers pays off in terms of efficiency, it makes the method's implementation more challenging than the straightforward full-grid approach. Based on the presented data and context, we can indeed identify some critical points that can help understand when the TT approach can be expected to perform better compared to the full-grid approach. This issue will be explored in our future works. However, it is worth noting that such critical issues are generally outweighed by the significant advantages in computational efficiency and storage requirements, particularly for larger problem sizes.

- *Initialization Overhead.* On the coarser grids, the TT method shows similar or occasionally slightly higher computational times compared to the full-grid approach. This suggests that some computational overhead occurs due to an initial TT decomposition and setup.
- *Memory Access Patterns.* The TT format, while more memory-efficient, may have less cache-friendly memory access patterns due to its smaller decomposed structure. This could explain why the computational advantage is not as pronounced for smaller problem sizes where cache effects may be less significant.
- *Additional Parameters.* The TT method introduces additional parameters such as the accuracy threshold for the rounding after normal arithmetic operations or inside the conjugate gradient iterations, and the ranks of the initial decomposition.

Finally, a particularly noteworthy result emerges from these calculations. The explicit Euler method is traditionally considered inefficient for parabolic problems due to the CFL stability condition, which requires the time step size  $\Delta t$  to scale with  $h^2$ . This constraint means that when the computational grid is refined by halving the spatial step size  $h$ , we must reduce  $\Delta t$  by a factor equal to 4, thus implying a fourfold increase in the number of iterations needed to reach a given final time  $T$ . The stability constraint is less restrictive for the implicit Euler and semi-implicit Crank-Nicolson methods, and it is a common practice to halve  $\Delta t$  when  $h$  is halved, just to keep the balance between the temporal and spatial approximation errors. However, a comparison of the absolute time costs (i.e., columns  $time_{TT}$ ) across all three time-marching schemes reveals an unexpected advantage of the TT format. Despite using an efficient preconditioned conjugate gradient method for the implicit and semi-implicit schemes, the computational cost per explicit Euler scheme iteration is much smaller in the TT format and remains competitive with implicit methods. This fact is in contrast with the usual (and accepted) notion regarding the relative efficiency of explicit versus implicit methods and deserve more investigation, which will be carried out in our future works.

## 7 Final Remarks

In this paper, we have developed and analyzed a tensor-train low-rank finite difference method for the efficient numerical solution of three-dimensional parabolic problems. Our approach combines the dimensional reduction capabilities of

the tensor-train format with classical finite difference discretization techniques, resulting in a powerful computational framework that significantly reduces both memory requirements and computational complexity.

The key innovation of our method lies in the tensorization process applied to traditional grid difference formulas, enabling the representation of solutions in a low-rank tensor-train format. This reformulation dramatically reduces the computational demands while maintaining accuracy, thereby extending the practical feasibility of solving three-dimensional problems that were previously intractable due to the curse of dimensionality. The integration of implicit and semi-implicit (Crank-Nicolson) time-marching schemes further enhances the method’s robustness and stability, providing a flexible framework which can be adapted to diverse problem settings.

Our comprehensive numerical experiments demonstrate the method’s superior performance compared to a conventional finite difference method’s design. Specifically, studying how the algorithm performs in the case of a rank-1 exact solution with a rank-1 initial approximation, we observe that the algorithm is rank-stable in the sense that there is no uncontrolled growth of the TT ranks. Additionally, we observe a substantial reduction in memory requirements while maintaining solution accuracy and a significant improvement in computational efficiency, particularly for large-scale problems. The robust performance across various test cases and problem parameters, also in the case of manufactured high-rank solutions, is promising for effectively handling challenging problem scenarios.

These results establish the practical viability of our approach for applications in computational physics, engineering, and scientific computing. The method’s demonstrated effectiveness in handling three-dimensional parabolic problems suggests its potential applicability to a broader range of scientific and engineering challenges, particularly in areas where computational efficiency is crucial. Future research directions may include the extension to a more general classes of partial differential equations with application to specific industrial and scientific problems.

## Acknowledgments

The LDRD-ER Project #20210485ER and the LDRD-DR Project #20250032DR funded the work of Dr. G. Manzini. The LDRD-ER Project #20210485ER also partially supported a three-week visit of Dr. T. Sorgente at LANL in August 2023. Los Alamos National Laboratory is operated by Triad National Security, LLC, for the National Nuclear Security Administration of the U.S. Department of Energy (Contract No. 89233218CNA000001). This work has been approved for public release and assigned the LA-UR number "LA-UR-25-22205". T. Sorgente is a member of the RAISE Innovation Ecosystem, funded by the European Union - NextGenerationEU and by the Ministry of University and Research (MUR), National Recovery and Resilience Plan (NRRP), Mission 4, Component 2, Investment 1.5, project "RAISE - Robotics and AI for Socio-economic Empowerment" (ECS00000035). G. Manzini and T. Sorgente are affiliated to the Italian Gruppo Nazionale Calcolo Scientifico - Istituto Nazionale di Alta Matematica (GNCS-INdAM).

## References

- [1] M. Bachmayr and K. Kazeev. Stability of low-rank tensor representations and structured multilevel preconditioning for elliptic PDEs. *Foundations of Computational Mathematics*, 20:1175–1236, 2020.
- [2] J. Ballani and L. Grasedyck. A projection method to solve linear systems in tensor format. *Numerical Linear Algebra with Applications*, 20:27–43, 2012.
- [3] R. Bellman. *Adaptive Control Processes: A Guided Tour*. Princeton University Press, Princeton, NJ, 1961.
- [4] M. Benzi. Preconditioning techniques for large linear systems: A survey. *Journal of Computational Physics*, 182(2):418–477, 2002.
- [5] F. Boyer and F. Hubert. Finite volume method for 2D linear and nonlinear elliptic problems with discontinuities. *SIAM Journal on Numerical Analysis*, 46(6):3032–3070, 2008.
- [6] F. Boyer, S. Krell, and F. Nabet. Inf-Sup stability of the Discrete Duality Finite Volume method for the 2D Stokes problem. *Mathematics of Computation*, 84:2705–2742, 2015.
- [7] D. Braess. *Finite Elements: Theory, Fast Solvers, and Applications in Solid Mechanics*. Cambridge University Press, 3 edition, 2007.

- [8] F. Brezzi, K. Lipnikov, and M. Shashkov. Convergence of the mimetic finite difference method for diffusion problems on polyhedral meshes. *SIAM Journal on Numerical Analysis*, 43(5):1872–1896, 2005.
- [9] S. Dolgov, B. Khoromskij, and I. Oseledets. Fast solution of parabolic problems in the tensor train/quantized tensor train format with initial application to the Fokker-Planck equation. *SIAM J. Sci. Comput.*, 34(6):A3016–A3038, 2012.
- [10] S. V. Dolgov. TT-GMRES: Solution to a linear system in the structured tensor format. *Russian Journal of Numerical Analysis and Mathematical Modelling*, 28(2):149–172, 2013.
- [11] K. Domelevo and P. Omnès. A finite volume method for the Laplace equation on almost arbitrary two-dimensional grids. *ESAIM: Mathematical Modelling and Numerical Analysis*, 39(6):1203–1249, 2005.
- [12] L. C. Evans. *Partial Differential Equations*, volume 19 of *Graduate Studies in Mathematics*. American Mathematical Society, Providence, Rhode Island, 2 edition, 2010.
- [13] B. Fornberg. *A Practical Guide to Pseudospectral Methods*. Cambridge Monographs on Applied and Computational Mathematics. Cambridge University Press, 1996.
- [14] G. H. Golub and C. F. Van Loan. *Matrix Computations*. Johns Hopkins Studies in the Mathematical Sciences. Johns Hopkins University Press, Baltimore, MD, 4th edition, 2013.
- [15] S. Goreinov, I. Oseledets, D. Savostyanov, E. Tyrtyshnikov, and N. Zamarashkin. How to find a good submatrix. In V. Olshevsky and E. Tyrtyshnikov, editors, *Matrix Methods: Theory, Algorithms and Applications*, pages 247–256, Singapore, 2010. World Scientific.
- [16] F. H. Harlow and J. E. Welch. Numerical calculation of time-dependent viscous incompressible flow of fluid with free surface. *Physics of Fluids*, 8(12):2182–2189, 1965.
- [17] V. Kazeev, I. Oseledets, M. Rakhuba, and C. Schwab. Quantized tensor FEM for multiscale problems: Diffusion problems in two and three dimensions. *Multiscale Modeling & Simulation*, 20(3):893–935, 2022.
- [18] V. Kazeev and C. Schwab. Quantized tensor-structured finite elements for second-order elliptic PDEs in two dimensions. *Numerische Mathematik*, 138:133–190, 2018.
- [19] B. Khoromskij.  $o(d \log n)$ -Quantics approximation of  $n$ -d tensors in high-dimensional numerical modeling. *Constr. Approx.*, 34(2):257–280, 2011.
- [20] T. Kolda and B. Bader. Tensor decompositions and applications. *SIAM Review*, 51(3):455–500, 2009.
- [21] D. Kressner, M. Steinlechner, and B. Vandereycken. Preconditioned low-rank Riemannian optimization for linear systems with tensor product structure. *SIAM Journal on Scientific Computing*, 38(4):A2018–A2044, 2016.
- [22] D. Kressner and C. Tobler. Krylov subspace methods for linear systems with tensor product structure. *SIAM Journal on Matrix Analysis and Applications*, 31(4):1688–1714, 2010.
- [23] R. J. LeVeque. *Finite Difference Methods for Ordinary and Partial Differential Equations: Steady-State and Time-Dependent Problems*. SIAM, 2007.
- [24] G. Manzini, P. Truong, R. Vuchkov, and B. Alexandrov. The tensor-train mimetic finite difference method for three-dimensional Maxwell’s wave propagation equations. *Mathematics and Computers in Simulation*, 210:615–639, 2023.
- [25] G. I. Marchuk. *Methods of Numerical Mathematics*. Springer-Verlag, New York, 2 edition, 1990.
- [26] L. Markeeva, I. Tsybulin, and I. Oseledets. QTT-isogeometric solver in two dimensions. *Journal of Computational Physics*, 424:109835, 2021.
- [27] Y. Morinishi, T. S. Lund, O. V. Vasilyev, and P. Moin. Fully conservative higher order finite difference schemes for incompressible flow. *Journal of Computational Physics*, 143:90–124, 1998.

- [28] M. K. Ng. *Iterative Methods for Toeplitz Systems*. Numerical Mathematics and Scientific Computation. Oxford University Press, New York, 2004.
- [29] I. Oseledets. Tensor-train decomposition. *SIAM, Journal on Scientific Computing*, 33(5):2295–2317, 2011.
- [30] I. Oseledets and E. Tyrtyshnikov. TT-cross approximation for multidimensional arrays. *Linear Algebra and its Applications*, 432(1):70–88, 2010.
- [31] I. V. Oseledets and S. V. Dolgov. Solution of linear systems and matrix inversion in the TT-format. *SIAM Journal on Scientific Computing*, 34(5):A2718–A2739, 2012.
- [32] J. B. Perot. Discrete conservation properties of unstructured mesh schemes. *Annual Review of Fluid Mechanics*, 43:299–318, 2011.
- [33] J. Shen, T. Tang, and L.-L. Wang. *Spectral Methods. Algorithms, Analysis and Applications*, volume 41 of *Srpinger Series in Computational Mathematics*. Springer, 2011.
- [34] J. C. Strikwerda. *Finite Difference Schemes and Partial Differential Equations*. SIAM series. SIAM: Society for Industrial and Applied Mathematics, Philadelphia, PA, 3 edition, 2007.
- [35] R. S. Varga. *Matrix Iterative Analysis*. Springer Series in Computational Mathematics. Springer-Verlag, Berlin, second edition, 2001.
- [36] H. K. Versteeg and W. Malalasekera. *An Introduction to Computational Fluid Dynamics: The Finite Volume Method*. Pearson Education, 2 edition, 2007.

## A Taylor expansions for first derivatives

We recall that

$$\begin{aligned} x_c(i_c) &= \frac{x_v(i_v) + x_v(i_v + 1)}{2} \quad \text{and} \quad h_x = x_v(i_v + 1) - x_v(i_v), \\ y_c(j_c) &= \frac{y_v(j_v) + y_v(j_v + 1)}{2} \quad \text{and} \quad h_y = y_v(j_v + 1) - y_v(j_v), \\ z_c(k_c) &= \frac{z_v(k_v) + z_v(k_v + 1)}{2} \quad \text{and} \quad h_z = z_v(k_v + 1) - z_v(k_v). \end{aligned}$$

so that, for three given integers  $m, n, p$  we can write

$$\begin{aligned} x_v(i_v) + mh_x &= x_c(i_c) + \Delta x(m) \quad \text{with } \Delta x(m) = (m - 1/2)h_x, \\ y_v(j_v) + nh_y &= y_c(j_c) + \Delta y(n) \quad \text{with } \Delta y(n) = (n - 1/2)h_y, \\ z_v(k_v) + ph_z &= z_c(k_c) + \Delta z(p) \quad \text{with } \Delta z(p) = (p - 1/2)h_z. \end{aligned}$$

From the definition of  $\Delta x(m)$ ,  $\Delta y(n)$ , and  $\Delta z(p)$  we note that  $(\Delta x(0))^2 = (\Delta x(1))^2$ ,  $\Delta x(1) - \Delta x(0) = h_x$ , and

$$\sum_{n=0}^1 \Delta y(n) = \sum_{p=0}^1 \Delta z(p) = 0.$$

We are now ready to perform the Taylor expansion of the vertex grid function values  $u_v(i_v + m, j_v + n, k_v + p)$  around the center of cell  $c(i_c, j_c, k_c)$ . In such expansion, we denote the first and second derivatives of  $u(x, y, z)$  with respect to  $x, y, z$  at the cell center as  $u_X = \partial u(x(i_c), y(j_c), z(k_c))/\partial x$ ,  $u_{XX} = \partial^2 u(x(i_c), y(j_c), z(k_c))/\partial x^2$ , etc. Since we assume that  $u_v$  is obtained by sampling  $u(x, y, z)$  at the mesh vertices, we find that

$$\begin{aligned} u_v(i_v + m, j_v + n, k_v + p) &= u(x_v(i_v) + mh_x, y_v(j_v) + nh_y, z_v(k_v) + ph_z) \\ &= u(x_c(i_c) + \Delta x(m), y_c(j_c) + \Delta y(n), z_c(k_c) + \Delta z(p)) \\ &= u_c + u_X \Delta x(m) + u_Y \Delta y(n) + u_Z \Delta z(p) \\ &\quad + \frac{1}{2} \left( u_{XX} (\Delta x(m))^2 + u_{YY} (\Delta y(n))^2 + u_{ZZ} (\Delta z(p))^2 \right) \\ &\quad + \frac{1}{2} \left( u_{XY} \Delta x(m) \Delta y(n) + u_{YZ} \Delta y(n) \Delta z(p) + u_{ZX} \Delta z(p) \Delta x(m) \right) + \mathcal{O}(h^3). \end{aligned} \tag{25}$$

Then, we sum over  $n \in \{0, 1\}$ , and  $m \in \{0, 1\}$  and we find that

$$\phi(m) := \sum_{n=0}^1 \sum_{p=0}^1 u_v(i_v + m, j_v + n, k_v + p) = 4u_c + 4u_X \Delta x(m) + [\text{second order terms}] + \mathcal{O}(h^3),$$

where  $\phi(m)$  is a suitably defined auxiliary function that depends on  $m \in \{0, 1\}$ , and, for simplicity, we collect all second-order terms in the squared bracket term  $[\dots]$ , which also depends on  $m$ . It is easy to see that this latter term is the same for  $m = 0$  and  $m = 1$ . Finally, we take the difference between the values of  $\phi(m)$  for  $m = 1$  and  $m = 0$ , and using the definition of  $\partial_x^c u_v$  we find that

$$4h_x \partial_x^c u_v = \phi(1) - \phi(0) = 4h_x u_X + \mathcal{O}(h^3),$$

which implies the first assertion in Eq. (8). We can prove the other two relations in (8) by repeating the same argument.

## B Taylor expansions for second derivatives

We substitute the Taylor expansion (25) in (10), which we rewrite here for convenience:

$$\partial_{xx}^c u_v(i_c, j_c, k_c) = \frac{1}{8h_x^2} \sum_{m=0}^3 \eta_m \sum_{n=0}^1 \sum_{p=0}^1 \xi_n \xi_p u_v(i_v - 1 + m, j_v + n, k_v + p),$$

where we recall that the coefficients  $\eta_m$  and  $\xi_n$  (or  $\xi_p$ ) take the values  $\xi_0 = -1, \xi_1 = 1, \eta_0 = \eta_3 = 1, \eta_1 = \eta_2 = -1$ . Then, we note that

- the terms with  $u(x(i_c), y(j_c), z(k_c))$  cancel out due to  $\sum_{n=0}^1 \sum_{p=0}^1 \xi_n \xi_p = 0$ ;
- the first derivatives in  $y$  and  $z$  cancel out due to the symmetry of  $\xi_n \xi_p$ ;
- the mixed derivatives cancel out for the same reason;
- the second derivatives in  $y$  and  $z$  only contribute to the generic error term  $\mathcal{O}(h^2)$ .

Therefore, we find that

$$\partial_{xx}^c u_v = u_{xx} + \mathcal{O}(h^2),$$

which prove the first assertion in (13). We can prove the other two relations in (13) by repeating the same argument.

## C Grid transformation

We briefly sketch the derivation of Eq. (16) to introduce the explicit transformation formulas for the first and second derivatives, which will be useful in the derivation of the finite difference formulas in both FG and TT formats. Let  $\tilde{u} : \tilde{\Omega} \rightarrow \mathbb{R}$  and  $u : \Omega \rightarrow \mathbb{R}$  be two functions related by the coordinate transformation, such that  $\tilde{u}(\tilde{x}) \equiv u(x)$  whenever  $\tilde{x} = \tilde{x}(x)$ . By applying the chain rule, we obtain the fundamental relation for the first derivative:

$$\frac{\partial}{\partial \tilde{x}} (\tilde{u}(\tilde{x})) = \frac{\partial u(x)}{\partial x} \frac{\partial x(\tilde{x})}{\partial \tilde{x}}.$$

This relation can be generalized to operate on any expression, yielding:

$$\frac{\partial}{\partial \tilde{x}} [\cdot] = \left( \frac{\partial x(\tilde{x})}{\partial \tilde{x}} \right) \frac{\partial}{\partial x} [\cdot].$$

For second derivatives, applying the operator twice results in:

$$\frac{\partial^2}{\partial \tilde{x}^2} [\cdot] = \left( \frac{\partial x(\tilde{x})}{\partial \tilde{x}} \right) \frac{\partial}{\partial x} \left( \frac{\partial x(\tilde{x})}{\partial \tilde{x}} \right) \frac{\partial}{\partial x} [\cdot].$$

A crucial property of these transformations follows from their inverse relationship. Since  $x(\tilde{x}(x)) = x$ , differentiating both sides yields:

$$1 = \frac{\partial x(\tilde{x}(x))}{\partial x} = \frac{\partial x(\tilde{x})}{\partial \tilde{x}} \frac{\partial \tilde{x}(x)}{\partial x},$$

which implies the fundamental inverse relation:

$$\frac{\partial x(\tilde{x})}{\partial \tilde{x}} = \left[ \frac{\partial \tilde{x}(x)}{\partial x} \right]^{-1}.$$

Substituting this result into the second derivative expression, we obtain our final form:

$$\frac{\partial^2}{\partial \tilde{x}^2} [\cdot] = \left( \frac{\partial \tilde{x}(x)}{\partial x} \right)^{-1} \frac{\partial}{\partial x} \left( \frac{\partial \tilde{x}(x)}{\partial x} \right)^{-1} \frac{\partial}{\partial x} [\cdot].$$

This formulation is particularly useful when the inverse transformation  $\tilde{x}(x)$  is known explicitly, as it allows us to express second derivatives in the physical domain in terms of derivatives in the reference domain.

## D Time integration: implementation details

Algorithm 2 details a single time step of the explicit Euler method from  $t^n$  to  $t^{n+1}$ . The input of the algorithm consists in  $u_v^{TT,n}$ , the TT grid function at the time step  $t^n$ , the right-hand side function  $f^{TT,n}$ , and the boundary function  $g^n$ , respectively evaluated at the internal and boundary vertices. The output consists in the updated TT vertex grid function  $u_v^{TT,n+1}$  at the next time step. The algorithm first enforces the boundary conditions. For all vertices residing in the ghost boundary frames described in Section 3.5, the auxiliary vertex grid function  $\bar{u}_v^{TT,n}$  is assigned  $g(\mathbf{x}, t^n)$ , the value of the boundary function evaluated at the vertex spatial coordinates  $x_v$  and current time  $t^n$ . Then, the algorithm stores the internal values of  $u_v^{TT,n}$  into the auxiliary field  $\bar{u}_v^{TT,n}$ . This preserves the solution at time  $t^n$  before the field  $u_v^{TT,n}$  is overwritten with the updated field  $u_v^{TT,n+1}$ . The algorithm computes the Laplacian of  $\bar{u}_v^{TT,n}$  at cell centers using the discretization formulas introduced in Section 3. This operation is denoted as  $\text{Compute Laplacian}(\bar{u}_v)$ . Then, the algorithm interpolates the cell-centered Laplacian  $\Delta^{c,TT}\bar{u}_v^{TT}$  at the mesh vertices resulting in  $\Delta^{v,TT}\bar{u}_v^{TT}$ . This step is necessary to obtain the Laplacian values at the same locations as the vertex grid function. Then, we compute  $\Delta t(\Delta^{v,TT}\bar{u}_v^{TT} + f_v^{TT})^n$ , the residual at each vertex, where  $f_v^{TT,n}$  is the TT representation of the right-hand side function evaluated at the mesh vertices and current time  $t^n$ , as detailed in Section 5. The vertex grid function is then updated by overwriting  $\bar{u}_v^{TT,n}$  with the new field  $u_v^{TT,n+1}$ . Finally, the algorithm performs the rounding operation to control the rank growth and assign the updated field to  $u_v^{TT,n}$ .

---

### Algorithm 2 Explicit Euler Method

---

**Input:**

- $f$ : right-hand side function on  $\Omega$
- $g$ : boundary function on  $\partial\Omega$
- $u_v^{TT,n}$ : TT vertex grid function at time  $t^n$

**Output:**

- $u_v^{TT,n+1}$ : TT vertex grid function at time  $t^{n+1}$

```

1: procedure EXPLICIT TIME MARCHING SCHEME( $f, g, u_v^n$ )
2:    $\bar{u}_v^{TT,n}(i_v, j_v, k_v) \leftarrow g(x(i_v), y(j_v), z(k_v), t^n) \quad \forall$  boundary vertex  $v(i_v, j_v, k_v)$  ▷ Assign BCs
3:    $\bar{u}_v^{TT,n}(i_v, j_v, k_v) \leftarrow u_v^{TT,n}(i_v, j_v, k_v) \quad \forall$  internal vertex  $v(i_v, j_v, k_v)$  ▷ Store Previous Values
4:    $\Delta^{c,TT}\bar{u}_v^{TT} \leftarrow \text{Compute Laplacian}(\bar{u}_v^{TT})$  ▷ Compute Cell-Centered Laplacian
5:    $\Delta^{v,TT}\bar{u}_v^{TT} \leftarrow \text{Vertex Interpolation}(\Delta^{c,TT}\bar{u}_v^{TT})$  ▷ Interpolate Laplacian to Vertices
6:    $f_v^{TT,n} \leftarrow g$  ▷ Compute forcing term
7:    $\bar{u}_v^{TT,n+1} \leftarrow \bar{u}_v^{TT,n} + \Delta t(\Delta^{v,TT}\bar{u}_v^{TT,n} + f_v^{TT,n}) \quad \forall$  internal vertex ▷ Update internal vertices
8:    $u_v^{TT,n+1} \leftarrow \text{rndg}(\bar{u}_v^{TT,n+1})$  ▷ Apply rounding procedure
9: end procedure

```

---

Algorithm 3 describes a single time step of the implicit Euler method for evolving a solution  $u_v^{TT,n}$  at time  $t^n$  to  $u_v^{TT,n+1}$  at time  $t^{n+1}$ . Like the explicit version, it takes the current solution  $u_v^{TT,n}$ , the right-hand side function  $f$ , and the boundary condition function  $g$  as inputs, and return the updated solution  $u_v^{TT,n+1}$  at the following time instant  $t^{n+1}$ . The auxiliary field in tensor-train format  $\bar{u}_v^{TT,n}$  is used to collect the boundary values at the current time step and to store the internal values of  $u_v^{TT,n}$  to preserve the solution at  $t^n$ . The key difference from the explicit method is that the implicit Euler method requires solving a linear system by applying the PCG to obtain  $u_v^{TT,n+1}$ . This step is represented in Algorithm 3 by the operation  $u_v^{TT,n+1} \leftarrow \text{PCG}(\bar{u}_v^{TT,n})$ .

Algorithm 4 presents the semi-implicit Crank-Nicolson method for evolving the solution  $u_v^{TT,n}$  at time  $t^n$  to  $u_v^{TT,n+1}$  at time  $t^{n+1}$ . This algorithm leverages both explicit and implicit Euler steps to achieve second-order accuracy in time. The inputs remain the same as for the explicit and implicit Euler methods: the current solution  $u_v^{TT,n}$ , the right-hand side function  $f$ , and the boundary condition function  $g$ . The algorithm initially sets the boundary conditions for the explicit step at the current time step  $t^n$ . Then, an explicit Euler step is taken with a half time step ( $\Delta t/2$ ) to compute an intermediate solution  $u_v^{TT,n+1/2}$  from the solution at  $t^n$ . Before the implicit step, the boundary conditions are updated to the values at the final time  $t^{n+1}$ . Finally, an implicit Euler step, also with a half time step ( $\Delta t/2$ ), is used to compute the solution  $u_v^{TT,n+1}$  from the intermediate solution  $u_v^{TT,n+1/2}$ . As in the implicit Euler algorithm, this step involves solving a linear system by applying the PCG method. By combining the explicit and implicit steps in this manner, the Crank-Nicolson method achieves second-order accuracy in time while retaining some of the computational advantages of the explicit method. The use of half time step  $\Delta t/2$  is essential for the correct implementation of the Crank-Nicolson



---

**Algorithm 3** Implicit Euler Method

---

**Input:**

- $f$ : right-hand side function on  $\Omega$
- $g$ : boundary function on  $\partial\Omega$
- $u_v^{TT,n}$ : TT vertex grid function at time  $t^n$

**Output:**

- $u_v^{n+1}$ : TT vertex grid function at time  $t^{n+1}$

```
1: procedure IMPLICIT TIME MARCHING SCHEME( $f, g, u_v^n$ )
2:    $\bar{u}_v^{TT,n}(i_v, j_v, k_v) \leftarrow g(x(i_v), y(j_v), z(k_v), t^n) \quad \forall$  boundary vertex  $v(i_v, j_v, k_v)$  ▷ Assign BCs
3:    $\bar{u}_v^{TT,n}(i_v, j_v, k_v) \leftarrow u_v^{TT,n}(i_v, j_v, k_v) \quad \forall$  internal vertex  $v(i_v, j_v, k_v)$  ▷ Store Previous Values
4:    $f_v^{TT,n+1} \leftarrow g$  ▷ Compute forcing term
5:    $b_v = \text{rndg}(\bar{u}_v^{TT,n} + \Delta t f_v^{TT,n+1})$  ▷ Compute RHS term
6:    $u_v^{n+1} \leftarrow \text{PCG}(b_v, \bar{u}_v^{TT,n})$  ▷ Solve Linear System using Preconditioned Conjugate Gradient
7: end procedure
```

---

scheme.

---

**Algorithm 4** Semi-implicit Crank-Nicolson Method

---

**Input:**

- $f$ : right-hand side function on  $\Omega$
- $g$ : boundary function on  $\partial\Omega$
- $u_v^{TT,n}$ : vertex grid function at time  $t^n$

**Output:**

- $u_v^{n+1}$ : vertex grid function at time  $t^{n+1}$

```
1: procedure SEMI-IMPLICIT TIME MARCHING SCHEME( $f, g, u_v^n$ )
2:   Set boundary conditions at  $t = t^n$ 
3:   Compute  $u_v^{TT,n+1/2}$  from  $u_v^{TT,n}$  using the explicit Euler scheme with time step  $\Delta t/2$ 
4:   Set boundary conditions at  $t = t^{n+1/2}$ 
5:   Compute  $u_v^{TT,n+1}$  from  $u_v^{TT,n+1/2}$  using the implicit Euler scheme with time step  $\Delta t/2$ 
6: end procedure
```

---